UCRL--21163

DE89 016653

TUBING WASTAGE IN FLUIDIZED-BED COAL COMBUSTORS
(TVA, 20 megawatt AFBC Pilot Plant)

By
Charles E. Witherell

Work Performed Under Contract No. W-7405-Eng-48
B & R Code AA-35-10-10-0

Prepared for
U.S. Department of Energy
Morgantown Energy Technology Center
Morgantown, West Virginia 26507-0880

Prepared by
Lawrence Livermore National Laboratory
Livermore, California 94550-0808

April 7, 1989

TABLE OF CONTENTS

Page

LIST OF TABLES

LIST OF ILLUSTRATIONS

TUBING WASTAGE IN FLUIDIZED–BED COAL COMBUSTORS[1] (TVA, 20 megawatt AFBC Pilot Plant)

1.0 ABSTRACT

Study of TVA tubing samples representing both wastage–susceptible and wastage–resistant tube banks has indicated a wastage mechanism similar to that identified in previously–studied tube samples from Grimethorpe (UK). Metallurgical differences between the two TVA tube banks were also observed that are believed relevant to their wastage response.

Wastage appears to occur through exfoliation of protective oxide scale caused by impingement and abrasion of fluidized bed materials. There is no evidence that chemical effects of elements such as sulfur or chlorine are responsible for or contribute to the wastage process.

The tube from the wastage–resistant tube bank, in contrast to the tubes that experienced wastage, formed an alloy–enriched layer at the scale/substrate interface that is apparently oxidation resistant and seems to protect the steel surface from mechanical impacts and abrasion of bed materials.

2.0 EXECUTIVE SUMMARY

Examinations of samples of carbon–steel evaporator tubes from TVA's 20 megawatt AFBC pilot plant were conducted by LLNL as part of a continuing program to identify wastage mechanisms and causes. These studies have revealed similarities between the TVA samples and samples previously studied from tube banks C and C–2 of the Grimethorpe PFBC unit.

Wastage along the undersides of in–bed evaporator tubes appears to be the result of localized exfoliation of protective oxide scale caused by impingement of bed particulates and aided by surface abrasion by bed materials that are being continuously forced upon and rubbed against the tube undersides by upward bed fluidizing motion. There are no indications that wastage is caused, or aggravated, by variations in bed chemical effects such as sulfur or chlorine content. All scales, both in wasted and non–wasted regions and in tubes that were and were not susceptible to wastage, contained calcium, aluminum, sulfur and silicon and traces of chlorine, potassium, and other elements. Concentrations of sulfur and chlorine were greater in non–wasted regions and favored the scale/substrate interface. Similar concentrations were also

[1]Work performed under the auspices of the U. S. Department of Energy by Lawrence Livermore National Laboratory, in collaboration with Morgantown Energy Technology Center, under contract number W–7405–ENG–48.

observed in tube samples that did not experience wastage. No attack attributable to such concentrations or other environmental variables – other than surface oxidation – was observed in any of the tube specimens examined.

A number of apparent metallurgical differences between the tubes of the two tubing banks, represented by the samples submitted, have been observed. These included differences in chemical composition of the steel itself, differences in their microstructure, in their indentation hardness at elevated temperature, and in the growth rate and appearance of their oxide scales. Principal differences were that steel from wastage–resistant tubes had higher levels of residual trace elements, was softer at elevated temperatures, had a more uniform and homogeneous microstructure, and formed a thinner duplex scale characterized by concentrations of chromium, silicon, nickel, and manganese at or near the scale/substrate interface. Steel from the tube bank that experienced wastage had very low levels of residual elements, was harder at elevated temperatures, had a banded microstructure, and formed a thicker and more porous scale that had no detectable concentrations of oxidation–resistant trace elements.

It is believed that the two steels, representing wastage–susceptible and wastage–resistant tube banks, were produced by different steelmaking processes, which account not only for the differences in the steels themselves but also in their response to FBC environments. All indications are that the wastage–resistant steel forms an alloy–enriched inner layer at the oxide scale–steel substrate interface that constitutes a protective shield or case that is firmly attached to the steel and that not only resists mechanical impacts and abrasion of bed materials but, because of its probable resistance to oxidation, also minimizes metal loss due to repetitive cycles of scale growth and exfoliation.

These findings suggest that continuing, confirming studies should be run and include preparation of experimental steel compositions representing various steelmaking alternatives. It is recommended that the resulting materials be characterized in laboratory tests followed by evaluation in actual operating combustors of test sections of full–sized tubes.

3.0 INTRODUCTION

This report covers results of examination of samples of evaporator tubing from the Tennessee Valley Authority (TVA) Atmospheric Fluidized Bed Combustion (AFBC) Pilot Plant in Padukah, KY. Examination of these samples is part of a program that LLNL is conducting in collaboration with the U. S. Department of Energy, Morgantown Energy Technology Center (METC) to identify the wastage mechanism or mechanisms responsible for metal loss that has occurred in in–bed evaporator tubing of fluidized–bed coal combustors.

4.0 PURPOSE

These studies are being undertaken to examine samples of evaporator tubes that have experienced metal loss during exposure to actual combustor conditions. To the extent available, the study includes both affected and unaffected tubes from different tube banks, different locations within a given tube bank, and representing a range of deterioration. The goal of this work is to formulate a plausible and coherent explanation of the wastage mechanism or mechanisms that is consistent with observed behavior and operating experiences.

5.0 BACKGROUND

Study of the TVA tube samples was conducted as a second round of examinations. The initial set, described in previous reports (1–2), was from Test Series 2 of the pressurized fluidized–bed combustor (PFBC) at Grimethorpe (U.K.), with samples from tube banks C and C–2. All tubes submitted for examination in that study had experienced wastage, although tubes modified through addition of protective longitudinal fins (C–2 tube bank, for example) exhibited less wastage than unmodified tubes. The Grimethorpe tubes had all been about 35 mm O.D. with a wall thickness of about 4.5 mm; the unprotected (non–finned) tubes were of carbon steel and the finned sample was of $2\frac{1}{4}\%$ Cr. - 1% Mo alloy steel.

All tubes received from TVA were of carbon steel, all had unmodified peripheries, and were substantially larger in diameter (about 54 mm O.D.) and with thicker wall (about 6 mm) than the previously–examined Grimethorpe tubes. The TVA samples were provided by Electric Power Research Institute (EPRI) site representatives who selected the materials submitted for this study. Information was provided on combustor locations for the samples submitted; however, details on relative wastage rates from one location to another within the combustor and as a result of differences in combustor operating parameters were not available. The information provided is summarized below.

6.0 MATERIALS AND PROCEDURES

6.1 Tubing Samples

Initially, two 6″ lengths of evaporator tubes from the second evaporator tube bank manufactured by Combustion Engineering, representing typically wasted surfaces, were sent to LLNL for examination. These tubes were identified as 27–A–1 and 27–A–4. According to the information provided (3), both sections were from Evaporator Pass 2; one from the bottom row (27–A–1) and the other from the top row (27–A–4). See Figure 1A. The sections were taken from locations referred to as "7A" (See Figure 1B).

Subsequently, two additional tubing samples were submitted. One of these was from the same Combustion Engineering tube bank as were the previous two samples, but from a different location of the tube bank (Row 1 of Serpentine #8). See Figure 2.

The second sample is of particular interest as it was from the original tube bank manufactured by Babcock and Wilcox (B&W), and was taken from the location shown in Figure 3. This tube sample was requested by LLNL to be included in the study as the B&W tube bank had extensive combustor exposure yet experienced minimal wastage. Therefore, it was considered useful to evaluate it to determine if there were differences in this apparently wastage–resistant material that might account for its superior response in the combustor. Table 1 summarizes information provided (4–5) with the tube samples with respect to combustor time, fluidized–bed conditions, and other details, as made available.

Figures 4A through 4D show surface appearance of the four tubing samples. In each figure, the four views represent successive 90 degree clockwise turns (from left to right as viewed from above) to show the complete periphery. The undersides of the tubes, as positioned in the combustor tube bank and that were subject to wastage (generally, from about a 4:00 to 8:00 o'clock position), had smoother texture and were more uniformly lighter colored (tan) than non–wasted regions. Non–wasted regions were generally of rougher texture and had a mottled dull–black appearance. The two regions were frequently separated by a fairly distinct line running longitudinally along the length of the tube. This is apparent in several of the photographs of Figure 4. Figure 5 shows cross–sectional profiles of the four tubes; extent of wall–thinning in regions of wastage is obvious.

According to information provided with the samples, the tubes were removed from the tube bank using a lubricated grinding wheel. The shorter lengths submitted for laboratory examinations were cut from the tubes using a hacksaw without lubricant.

6.2 Examination Methods

6.2.1 Visual Inspection. As–received appearance of the samples was photographically documented before other inspection steps were taken (Figure 4). This included examination of transverse cross sections to observe extent and location of wastage (Figure 5). The tubing fireside surfaces were examined visually at magnifications up to about 20X to reveal general surface features, textures, coloration, presence and appearance of deposits or scales, and overall condition.

Scanning electron microscopy (SEM) was used extensively to characterize and compare features of both wasted and non–wasted surfaces and wastage–transition regions. Tubing cross–sections were also examined using SEM to determine scale morphology and thickness, scale/interface features, extent of preferential attack, if any, and the role of microstructure in the wastage process, if any.

The specimens were prepared using the same general techniques as reported previously (6). This included precautions to avoid contaminating surfaces with cutting lubricants and polishing media, and polishing of cross–sections without water to avoid the possibility of leaching water–soluble species. Special preparation techniques were required for preserving the integrity of surface scales for examinations of cross–sections, and these are described in the report previously cited. As before, mounted and polished cross–sections intended for SEM work were pre–sputter–coated with a conductive layer of either carbon or a gold/palladium alloy.

6.2.2 Chemical Testing. Various kinds of tests were conducted to determine chemical composition and included surface analyses as well as conventional gravimetric analyses. Surface analyses were conducted to identify the composition of surface films, deposits, scales and other features. These used such analytical techniques as Auger electron spectroscopy (AES) (with progressive ion milling), X–ray photoelectron spectroscopy (XPS), electron microprobe (EMP) X–ray fluorescence (XRF), and energy–dispersive spectroscopy (EDS) in conjunction with SEM equipment.

Chemical compositions of the tubing steels also were determined using standard quantitative methods. These were performed on clean samples cut from the tubes and after both water–side and fireside surfaces had been machined dry to a depth sufficient to remove all traces of scale.

6.2.3 Physical Testing. Several types of physical tests were conducted in the course of the examination. On selected samples, extent of dislocation density, indicative of surface deformation during combustor exposure, was evaluated using transmission electron microscopy (TEM) techniques.

TEM specimens were prepared for both wasted and non–wasted regions. For wasted regions, specimens were also prepared for several subsurface locations to investigate depth effects. These depth locations were established by progressively electropolishing inward for selected periods of time, then thinning the specimens from behind to permit TEM examination. Reference specimens, representing midwall microstructure, were included in all TEM measurements to establish the condition of tubing metal in its as–produced state.

Evaluation of elevated temperature indentation hardness was conducted on specimens that were prepared similarly to those for determining all–metal chemical composition: that is, on tubing sections that had all scale removed by dry machining. After machining, the resulting rings were cut to provide $1/2''$ long circular segments from the approximately $3/8''$ wide tubing cross–sections. These were surface–ground to obtain flat uniform samples with parallel sides to facilitate obtaining accurate hardness determinations.

After cleaning, specimens of each tube were hardness tested (Rockwell B scale) at room temperature, duplicates were tested at elevated temperatures from 400 F (204 C) through 800 F (427 C) at 100°F (56 C) intervals and at 840 F (450 C). The specimens were heated in the testing apparatus to the desired test temperature, then held at least 5 minutes at that temperature before testing. Protective argon atmosphere was circulated throughout the test chamber during all elevated temperature tests. Rockwell B hardness measurements were performed on one specimen of each tube sample at each temperature, with at least 5 hardness determinations made for each set of conditions.

6.2.4 Oxidation Tests. Selected tubing samples also were subjected to laboratory oxidation tests to observe effects of differences in microstructure and chemical composition of the tubing samples upon elevated temperature oxidation behavior. Machined tubing segments free of scale and oxide were placed in individual porcelain boats and heated in still air to 450 C (840 F) in a laboratory electric oven and

held at that temperature for 100 hours. After furnace–cooling to room temperature, cross–sections were prepared for examination by optical metallography and SEM and chemical analysis by EDS/EMP methods.

7.0 RESULTS

7.1 Surface Characterization

7.1.1 Micromorphology. SEM examinations indicated that all fireside surfaces of the as–received tubes, wasted as well as non–wasted, contained scales and scale–like deposits. Typical appearance of surfaces in both regions at the same general magnification is shown in Figure 6 through 9 for all four tubing samples. As shown in these figures, wasted surfaces are generally smoother than non–wasted surfaces of the same tubing sample. However, there are differences in surface roughness and texture from tube to tube, as are apparent upon comparing Figures 6 and 7. This may be related to the particular location of the tube in the combustor.

For example, non–wasted surfaces of tubes 27–A–1 and 27–A–4 (Figure 6 and 7, respectively) have similar appearance, with rough heavy–appearing scales, showing evidence of fractures and exfoliated layers. Wasted regions are quite different in appearance – both from each other and from non–wasted regions. The wasted region of 27–A–1 (Figure 6) has a fine granular texture that appears to be a coating of agglomerated particulates that are adhering to the tubing surface. This is more clearly evident in the higher magnifications of Figure 10. Wasted surfaces of tubing sample 27–A–4 do not have this appearance. Figure 11 shows the appearance of the wasted region at a higher magnification than Figure 7. While the scale appears more dense, there are some scattered particulates similar to those in Figure 10 on the surface. Also, cracks in the scale are present in these areas devoid of the coating of fine particles.

Surface appearance and texture of the scales on tubing 8–1 again were different. Here, the surfaces are generally smoother and not as coarse as tubing samples 27–A–1 and 27–A–4, although the tendency for the wasted region to be smoother than the non–wasted region is observed in this tube, as well. Combustor location may be related to the differences in appearance of this tube in contrast to 27–A–1 and 27–A–4. In this respect, it may be relevant to note that tubing 8–1 had somewhat different exposure in the combustor (see Table I), including use of different coals for the last exposure period.

Tube 10–3–105, that had minimal wastage, had generally the same surface appearance around its periphery and typical appearance is shown in Figure 9. The surface is similar in appearance to other non–wasted regions in that it has a coarser texture with evidence of flaking or exfoliation in scattered regions. This tube bank had much longer combustor exposure than the other three tubes and this exposure involved the use of different coal than was used for the combustor runs involving the other three tubes.

7.1.2 Chemical Analyses. During the SEM examinations described in the previous section, energy dispersive spectroscopy (EDS) x-ray fluorescence (XRF) determinations of chemical composition were made on these surfaces. The areas scanned for the basic analyses were roughly that of the SEM photomicrographs shown in Figures 6 through 9. Because this analytical method cannot detect oxygen, but cations only, no attempt was made to obtain quantitative values, as these scales are oxides, predominantly, possibly mixed with other oxygen-containing compounds.

The analytical evaluations disclosed the same general chemical composition of scale on all surfaces, although there were minor differences that may be significant. All scales were predominantly iron, with minor amounts of calcium, sulfur, silicon and aluminum. Traces of chlorine, potassium, manganese, titanium and chromium were also detected in some samples.

There was significantly higher calcium content in the scale of wasted surfaces of tubing 27–A–1 than on non–wasted surfaces of the same tube. This seems to be related to the heavy distribution of fine particulates on these surfaces, (per Figure 10 and lower photo of Figure 6), as these particles had high calcium content. Wasted surfaces of this tubing sample also had titanium present, although none was detected on non–wasted surfaces or on either region of any of the other samples. Small amounts of aluminum, silicon, sulfur, chlorine and manganese were present on both wasted and non–wasted surfaces. Chlorine and manganese levels were higher in non–wasted regions of this tube sample (27–A–1).

Surface scale on tube sample 27–A–4 had a composition similar to that of sample 27–A–1, but with higher aluminum and silicon levels and lower calcium.

In sample 8–1, the wasted region had higher calcium and silicon contents than did the non–wasted region. In the non–wasted region of sample 8–1 chlorine was noticeably higher, and the sulfur level slightly higher. In comparison with samples 27–A–4 and 27–A–1, the scale of sample 8–1 had higher sulfur content (in both wasted and non–wasted regions) and, in the non–wasted region, higher chlorine. The higher chlorine level in the non–wasted region of sample 8–1, in contrast to that of samples 27–A–1 and 27–A–4, may be due to the fact that, for its entire exposure, sample 8–1 was subjected to Pyro coal having a chlorine content of 0.30%; while samples 27–A–1 and 27–A–4 had two test periods (#7 and #8) which used Warrior coal having a 0.05% chlorine content, although their final test period, #9, again used Pyro coal (0.30% chlorine).

In sample 10–3–105, sulfur and silicon levels in the surface scale were higher and calcium content lower than in either region of the other three tubing samples. There was a fairly distinct EDS peak for chlorine (although lower than that of the non–wasted region of sample 8–1). However, Sample 10–3–105 is the only sample of the four studied in this phase of the program that gave a definite indication of chromium in the surface scale.

7.2 Cross–Section Characterizations

7.2.1 Scale Appearance. The scales formed on the steel tubes were continuous around the entire periphery, although their thickness varied from one region to another. The scales were predominantly Fe_3O_4 with a hard, dense, and gray–colored appearance. There was almost always a layer or band of Fe_2O_3, generally at or near the outer surface. This material had a more grainy or porous–appearing texture with a red–brown (rust) color. In some regions there were distinct layers of what appeared to be Fe_2O_3 that had followed cracks in the Fe_3O_4 layer.

The scales were complex and non–uniform in texture, density and thickness around the periphery of a given tube region although there were dominant features associated with particular regions. The scales were frequently cracked, with crack directions running both longitudinally and transversely to the plane of the scale layer.

In non–wasted regions, generally at the top–side of the tube as positioned in the combustor, the surface scale was usually thicker and more continuous than at the lower (roughly 5:00 to 7:00 o'clock) region where wastage occurred. Also, there was a tendency for the scale/metal interface to be smoother in non–wasted regions and more ragged and irregular in wasted regions. In wasted regions, or at the tubing undersides where wastage occurred, there also was evidence of mechanical deformation of the tubing metal just below the scale/metal interface. In this series of tube specimens, this was observed only in etched samples at high magnification and sometimes required oblique lighting for its visual resolution. Deformation was not observed in non–wasted regions, only in wasted regions or at the underside locations where wastage occurred (or would have occurred in non–wasted samples).

Figures 12 and 13 are optical photomicrographs that show typical appearance of surface scales on tubes that experienced different wastage response in the combustor. Figure 12 shows tubing sample 8–1 which experienced considerable wastage in just under 4,000 hours; whereas Figure 13 shows tubing sample 10–3–105 from another tube bank that had only minimal wastage after more than 13,000 hours. In Figure 12, different magnifications were used to preserve detail without excluding pertinent areas. The difference in scale thickness from one region to the other (thicker in non–wasted region) is apparent when magnification differences are taken into account. Also note that the oxide in either region has not preferentially attacked any particular microstructural region. Slight deformation is apparent in some locations (photo center) of the wasted region although it is difficult to discern in photographs.

It is of interest to note that the scale thickness of tube sample 10–3–105, shown in Figure 13, is thinner than that of the non–wasted region of Sample 8–1 (Figure 12) but heavier than that of the wasted region of the same sample. Also, despite the favorable combustor response of tube 10–3–105, there is evidence of deformation having occurred along the undersides. Deformation is evident in the upper photomicrograph of Figure 13 in the metal substrate just below the scale interface. The scale/substrate interface of this tube sample otherwise resembled that of non–wasted regions of the other three samples in that it was smoother and not as irregular and ragged as it was in wasted regions of those other samples that had been susceptible to wastage.

7.2.2 Scale Compositions and Elemental Distributions. Previous studies of chemical compositions of surface scales indicated little difference from region to region of the same tube and from tube to tube within the combustor (7). In general, it was found that the bulk of the scale was Fe_3O_4 (magnetite), an oxide, containing aluminum, silicon, sulfur and calcium. It extended from the interface with the steel substrate outward. At the immediate fireside surface, there was a thin layer of Fe_2O_3 (hematite), also containing aluminum, silicon, sulfur and calcium in varying amounts, depending upon the tube location and region of that tube. Initial studies on the tubes of this study, as well, indicated the same general scale compositions; therefore, attention was focused upon determining elemental distributions.

The most informative analytical method to determine relative intensities of elemental distributions throughout the scale and along the interface of cross sections is x-ray fluorescence (XRF) element mapping. These were carried out using the EMP instrument. For each set of measurements, a secondary electron image (SEI) was first obtained to provide visual orientation and morphological and textural details of the scalar deposit and its interface along the substrate. Then, without repositioning or changing magnification, the same surface was scanned for individual elements of interest. In this case, the elements were sulfur, chlorine, potassium and calcium (K-alpha lines for each). These measurements were carried out in some detail for two samples, 27-A-4 and 10-3-105, representing a tube that experienced wastage (27-A-4) and one that resisted it (10-3-105). Two principal regions of each tube sample were scanned: (a) the wasted (underside) region of sample 27-A-4 and the corresponding combustor position of sample 10-3-105, even though it had experienced no wastage; and (b) the non-wasted (topside) region of sample 27-A—4 and the corresponding combustor position of sample 10-3-105. The results are shown in Figures 14 through 17 with one set of elemental maps for each region of the two tube samples.

For tube sample 27-A-4 (Figures 14 and 15), elemental concentrations generally are more intensive in non-wasted regions. This was observed consistently on all analytical runs; although preferred locations for the various elemental concentrations do not change from wasted to non-wasted region. That is, sulfur and chlorine seem to concentrate preferentially along the scale/metal interface while potassium and calcium are more diffused throughout the scale. Sulfur, however, was the dominant element of the four with high concentrations in the scale along the interface and within pores and crevices. This was always much more pronounced in non-wasted regions as shown by a comparison of Figures 14 and 15 (non-wasted and wasted regions, respectively).

These trends were generally the same for the same two corresponding regions of tube sample 10-3-105 (Figures 16-17). However, in that tube, the chlorine concentration (along the interface) in the scale at the underside was greater than it was at the topside, or in either region of tube sample 27-A-4. Potassium, also, tended to concentrate more along the interface at the underside and more, again, than was observed in Sample 27-A-4. Sulfur, however, was heavily concentrated along the interface at the topside and more diffused in the scale at the bottomside (although preferring pores and crevices), as in sample 27-A-4. As noted in previous studies, sulfur and calcium concentrations are not associated with one another.

During EDS studies of these samples, particularly while exploring the chemical composition along the scale/substrate interface, an enrichment of various elements was observed in all specimens in a thin (1–2 microns) layer right at the interface. For most specimens, this narrow region usually had higher silicon and aluminum, higher manganese in some and, in tube 10–3–105, higher chromium.

7.2.3 Microstructure. Examinations of metallographically–prepared specimens of steels from the two tube banks revealed a number of differences. The most pronounced was the banded microstructure of the C–E tubes and a more uniformly distributed microstructure in the B&W tube. The pearlite bands in the C–E steel were generally parallel but undulating, and spaced fairly equidistant from one another by the separating ferrite matrix and, for the most part, interconnected. They tended to run in circular concentric patterns around the tube and parallel to its inner and outer cylindrical surfaces. They also tended to follow ferrite grain boundaries, and the pearlite lamellae were generally distinct. The ferrite matrix in the C–E steel was exceptionally clean and generally featureless with virtually no non–metallic inclusions. Grain size was somewhat larger than in the B&W tube.

Besides being more uniformly distributed, the pearlite islands in the microstructure of the B&W steel were not interconnected but, as in the C–E steel, tended to favor ferrite grain boundaries, yet were usually well separated and surrounded by the ferrite matrix. The pearlite lamellae, again, were distinct and had not become decomposed. Unlike the C–E steel, the ferrite matrix of the B&W steel had a moderate distribution of fairly large non–metallic inclusions scattered throughout the microstructure. Microstructures of the two steels at the same magnification are shown in Figure 18.

7.3 Chemical Compositions of Tubing Metal

The compositional differences of the interface layer prompted comprehensive quantitative analyses to be conducted in an attempt to determine whether these effects were reflections of tubing metal composition or possibly brought about by combustor environmental variables. Of interest in these analyses were the compositions of the tubing metal itself, independent of effects of combustion environments. The resulting analyses for tubes from the two tube banks represented in the samples studied are listed in Table 2. Only tube sample 27–A–4 of the second tube bank was analyzed, as it was understood to be from the same lot of tubing as other tubes of the same bank (i. e. 27–A–1 and 8–1).

Although the carbon contents of the two steels are remarkably similar, other differences in background trace elements may be significant. Chromium content of sample 10–3–105, although not high at 0.12%, is more than an order of magnitude greater than that of sample 27–A–4. Other differences also are apparent: among others, aluminum, copper, molybdenum, nickel, and sulfur, all are notably higher in tube 10–3–105.

It is evident upon comparing the two steel compositions, that different steelmaking processes were used in producing these two lots of steel. It is suggested from the

very low levels of normally-found trace elements in tube sample 27-A-4 that either virgin melt charges were used or the melted heat was blown with oxygen or other gas combination to oxidize almost all trace elements before making the final principal alloying additions of carbon and manganese. Whichever it was, it is apparent that the steel of tube sample 10-3-105 is not a product of the same treatment.

7.4 Transmission Electron Microscopy (TEM)

As described in reports of previous studies (7), TEM examinations can provide indications of mechanical deformation of the tubing metal. This information is useful in determining metal loss mechanisms (i.e. whether external impacts played a role in the wastage process).

It was originally intended to evaluate tube samples 8-1 and 10-3-105, representing tubes that were, respectively, susceptible to and resistant to wastage in the combustor. And it was desired to evaluate tube metal in three regions of each tube sample: (a) wasted region, (b) non-wasted region, and (c) reference material from the tube wall located the same radial distance from the inside (water-side) surface as the wasted surface. This latter material would be taken from the non-wasted portion of the tube wall and would indicate the TEM microstructure of material unaffected by the combustor environment.

Attempts to obtain suitable TEM samples from all three regions of both samples were unsuccessful, largely because of the non-uniform and pitted condition of most fireside surfaces. This was particularly evident in surfaces of sample 10-3-105 and the unwasted region of sample 8-1 - all regions where wastage had not occurred or was minimal.

The problem in obtaining suitable TEM specimens from these surfaces was that the large number of micro-pits along the metal substrate just below the inner layer of scale in these regions not exposed to the erosive or scouring effects of bed particulates prevents obtaining intact, sound and uniformly thinned wafers for TEM study. Micro-pits cause premature perforation during preparation of the samples, preventing meaningful test results. The result of this was that useable specimens, suitable for TEM examination, were obtainable only from the relatively smooth wasted region of sample 8-1 and the reference region of that sample; although some indications were obtained, after many attempts, for the non-wasted surface of sample 8-1.

Photomicrographs of TEM microstructures of these three regions are shown in Figure 19. There are a number of observations to make in evaluating these microstructures. One, is that the photomicrographs at the center and left side represent metal from not only the same tube sample but from the same location within the tube wall (same radial distance from tube bore or central axis). The left-hand photo represents material at the wasted surface and the center photo represents material in its as-produced state (the original state of the metal at the same location as that shown in the left-hand photo, but before exposure to FBC environments). The difference in density of dislocations - an indication of extent of mechanical deformation - is clearly evident. This indicates that the wastage process involves, at least to some degree, mechanical surface forces that produce deformation.

The right–hand photo, representing material at the top–side, or non–wasted region, of the same tube sample, exhibits more dislocations than mid–wall reference material but considerably less than material at the wasted surface.

7.5 Hot Hardness Survey

These tests also showed differences in the two steels. The average indentation hardness values obtained are plotted in Figure 20. As shown, the B&W tube steel is softer over the entire test range than the C–E steel. Although room temperature hardness of the two steels is similar, hardness of the B&W steel drops off with increasing temperature to 400–500 F while that of the C–E steel remains nearly constant over the same temperature range. Above about 400 F, hardness of the C–E steel drops gradually as that of the B&W steel remains unchanged (with a slight increase at 700 F, possibly due to strain–aging as a result of the higher levels of residual elements), but decreases thereafter. While the hardnesses of the two appear to converge at temperatures above about 900 F, and may do so, a difference between them persists throughout the entire range of tube operating temperature.

7.6 Laboratory Oxidation Tests

The principal purpose of these experiments was to determine if the compositional and microstructural differences between the two tubing steels would affect oxidation response in a simple oxidized atmosphere of still air, in contrast to the complex FBC environment. If so, it would help to confirm that the differences that were observed in these two steels are in some way responsible for their different behavior in the combustor. Besides this, if such differences are observed in simple laboratory tests, such a finding would assist in identifying key parameters because of fewer obscuring variables than exist in a coal combustor. Also, if lab tests provide reliable indications of scale formation, consistent with combustor response, as a function of tube chemical composition and microstructure, such tests would constitute a much more effective and direct means for evaluating these differences than conducting full–scale FBC tests.

The oxide scales formed on the two steels during the 100–hour laboratory exposure at 450 C (842 F) had significant differences, as shown in Figure 21. The scale on the C–E (tube sample 8–1) steel was not only thicker, but more porous and appeared to grow directly from the substrate without an intervening sub–layer. Scale on the B&W steel (tube sample 10–3–105) was thinner, less porous, and had a distinctive, thin, pebbly–appearing band located a micron or two from the steel substrate. This band was fractured continuously along its entire length; although this fracture may have occurred during preparation of the sample cross–sections. Details of the scale interface are more clearly evident at the higher magnification of the scanning electron micrographs of Figure 22.

EDS and EMP traces run transversely across the scale and the scale/substrate interface of both steels revealed some significant differences between them. Traces run at various locations of the specimen at high levels of beam resolution repeatedly

showed a chromium peak in the vicinity of the pebbly–appearing inner band of the scale and inward toward the steel substrate in the B&W steel (tube specimen 10–3–105), as well as a corresponding sharp increase in silicon content.

Similar traces run on the C–E steel (tube specimen 8–1) showed a sharp peak of silicon, but no chromium. EDS estimates of elemental concentrations in the B&W steel at or near the rich/substrate interface indicated a silicon level of 5–10%, chromium, nickel, and manganese levels of 3–4%, and calcium content just under 4%. Because the analytical method does not detect oxygen, and since these deposits are oxides, actual levels of these elements would be roughly about half of these values. Other elements, such as molybdenum and sulfur, may also have been concentrated at the same location, but their spectral lines were obscured by the almost–superimposed gold/palladium lines from the sputter–coated conducting deposit. For the C–E steel, there was no detectable chromium, nickel or calcium; indicated silicon concentration was about 6% (again, ignoring the presence of oxygen), and very low manganese content (less than 0.1% indicated).

8.0 DISCUSSION

8.1 Wastage Mechanisms

It is apparent from the presence of scales and scale–like deposits on all tubing surfaces – wasted as well as non–wasted – that the wastage process involves more than the simple erosion or wearing away of the tube wall by impinging bed particulates. This is consistent with early predictions that particle velocities in FBC environments were insufficient for erosive wear of metal surfaces (8–9). Nevertheless, metal loss, or wastage, is obviously occurring during combustor operation and it is concentrated at the undersides of tubes that are subject to upward impingement of bed matter; the impingement forces being produced by injection of fluidization gas (air) at the bottom of the bed causing bed particulates to be carried upward or lifted until they encounter an obstruction – in this case, the in–bed evaporator tubes where they strike – or their upward path is impeded by – the tube bank array. Even though impingement velocities are low, it is obvious from knowledge and observation of fluidized bed action that bed matter is continually being forced upward against the tube undersides.

While these upward forces and particulate velocities may not be sufficient to remove metal by repetitive plowing and cutting of the tube surface – processes typical of classical erosion; they may be sufficient to abrade or scour away oxide scale. And this seems to be the mechanism of metal loss, as summarized below:

(a) Scale forms on all exposed steel tube surfaces. At these temperatures under normal conditions, (i.e. as in non–wasted regions where the scale has not been mechanically disturbed), it is apparently protective such that the rate of oxidation of the carbon steel tube diminishes exponentially as the scale thickens until oxidation rate becomes very low or essentially nil (10–11). Under these conditions, intact scale should offer virtually indefinite protection to the steel tube. If it should become damaged, it is self–healing; however, regenerated scale will form at the expense of tube wall, as the scale is mostly iron oxide.

(b) If the protective surface scale is repeatedly damaged, it would be expected that it would repeatedly attempt to heal itself in the region of the damage. But this would result in localized loss of tubing metal and, if allowed to continue, thinning of the tube wall would occur. In an extreme situation where the normally protective surface scale is continuously rubbed off or abraded away locally, oxidation rate of that steel surface would be very high and, accordingly, so also would metal loss in that region (12)(13).

(c) If continuous surface abrasion of the protective scale is also accompanied by frequent or repetitive impacts of bed particles of sufficient hardness, size, and mass; exfoliation of the scale would be accelerated. Under these conditions, scouring or abrasion forces may not need to be high enough to dislodge the scale but simply enough to provide clean, fresh metal where the scale has exfoliated from or flaked off the tube surface. This condition would constitute a very favorable surface for oxidation and, if the scale loss/regrowth cycle continues, oxidation at a high rate.

All indications are that the latter is probably the prevalent mode of scale loss, in light of the evidence (per TEM examinations) of metal deformation occurring in regions of tube wastage. However, there are indications that impingement of bed particulates does not, of itself, mean that high rates of wastage will always occur. The undersides of tube sample 10–3–105 showed evidence of surface deformation; yet, the tube did not experience any significant wastage in the combustor over a period of nearly 14,000 hours.

In summary, then, metal loss appears to be the result of localized exfoliation of protective oxide scale caused by impingement of bed particulates and aided by surface abrasion by bed materials that are continuously rubbed against the tube undersides by upward bed fluidization forces. Since fluidized beds involved in the wastage process are of the "bubbling–bed" type, tube wall abrasion may be related to bubble passage. That is, as the wakes of passing bubbles collapse, higher-than-normal impingement forces would be expected to occur, causing increased pressure to be imposed by bed material against the tube wall (13–14). And this would be expected to result in a higher rate of scale exfoliation.

If, in fact, wastage of in–bed evaporator tubes occurs by the suggested mechanism or series of occurrences, it would not be difficult to reconcile differences in degree of tube wastage from one location of the bed to another. For example, locations of air injection nozzles and coal feed ports can affect local bed fluidization conditions, and placement of tubes in the bed can influence bubble paths and streaming preference. All of these would have an effect upon the forces, directions and mass of bed matter that is contacting given tube surfaces at any time. And this could directly affect scale retention; that is, whether it remains protective or is exfoliated, the rate at which exfoliation occurs, and the degree to which the scale is permitted to re–form. All of these characteristics would affect wastage rate.

It has been suggested from time to time that chemical variables specific to individual fluidized–beds govern whether tube wastage does or does not occur. These

variables could result from differences in chemical composition of the coal used, grades of sorbent added, or due to differences in combustion efficiency or localized temperature gradients that could affect chemical activity. Chlorine and sulfur, and sometimes potassium and other elements, are mentioned in this context (15–17).

In the tubes examined in this study, all scales were found to contain calcium, aluminum, sulfur and silicon and traces of chlorine, potassium and other elements. It is believed significant that these elements were found in both wasted and non-wasted regions and, in some cases, their concentrations seemed to correlate with the chemical compositions of coal used. The fact that EDS analysis of surface scale of tube 10–3–105 (from the B&W tube bank that resisted wastage) showed a distinct peak for chlorine would suggest that the presence of chlorine, per se, does not make FBC tubes susceptible to wastage.

In examinations of cross sections to determine elemental distributions, concentrations of sulfur and chlorine were always greater in non-wasted regions and favored the scale/substrate interface. This is understandable, as scale in non-wasted regions is virtually undisturbed and apparently is at its equilibrium state for the temperature and chemistry of the fluidized bed. Under these circumstances, inward diffusion and development of compositional gradients would be expected to take place unhindered by scale loss or other disruptive influences. Under the operating conditions involved, there was no apparent detrimental effect of concentrations of sulfur and chlorine along the scale interface. This is most evident in examinations of scales at non-wasted surfaces. It is further borne out by observations of similar elemental concentrations in the tube sample that did not experience wastage; even at the undersides which, presumably, were exposed to upward impingement of bed particulates as were tubes of the other tube bank that did experience wastage.

It is of interest in the context of identifying tube wastage mechanisms to note that the tubes of this study that experienced wastage were similar in many respects to tubes examined in a previous study. In that study, tubes from Test Series 2 (tube banks C and C-2) of the National Coal Board (IEA Grimethorpe) Ltd. facility in the U.K. also were examined to determine wastage mechanisms. A report describing the results of that study (18) concluded that continual exfoliation of the normally-protective oxide scale was probably responsible for a major portion of the tubing wastage. There were also indications of direct metal loss occurring through a series of events wherein repeated formation and exfoliation of surface oxides produced on irregular metal interface that was mechanically deformed during combustor operation. Cold-worked metal protrusions, or platelets, on the roughened surface readily fractured from the tubing wall and were lost into the bed.

While wasted regions of the TVA tubes of the present study were very similar in appearance and chemical composition to the earlier Grimethorpe tubes, the indications are that the Grimethorpe tubes were subjected to conditions that produced higher rates of exfoliation than those to which the TVA tubes were exposed. Both sets of tubes bore evidence of mechanical deformation at the immediate surface of the steel substrate; however, there was no indication that TVA tube conditions produced the extent of cold-working of surface protrusions that was observed in tubes from the Grimethorpe PFBC Series 2 experiments. No flattened metal particles, flakes, or

platelets were found at or along the surfaces of any of the TVA tubes, suggesting that conditions were not as aggressive as in the Grimethorpe unit. And wastage rates at Grimethorpe were much greater, with tube bank C experiencing metal loss rates as high as 0.5 to 1.5 mm per thousand hours.

8.2 Metallurgical Influences

If it was not known that some tube banks survive FBC environments for extended periods of operation while others experience wastage under apparently the same conditions, it might be reasonable to assume that control of the problem must come from the direction of changing fluidization conditions, modifying the chemistry of the FBC environment, or shielding vulnerable surfaces of the tubes in some way to eliminate or substantially reduce those forces and conditions that cause scale exfoliation. As noted above, tube wastage has not been a uniform occurrence throughout a combustor but, in a given unit, wastage has favored various locations and fluidization conditions. This suggests that there is some optimal combination of combustor design and operating conditions that would correct the problem.

Undoubtedly, all of this is true, and it is prudent, reasonable and desirable to take any such steps that seem warranted in an effort to minimize, if not overcome, the wastage problem. Notwithstanding this, there is additional evidence in this study that relief may be obtainable from yet another direction, that is through optimizing metallurgical characteristics of the carbon steel tubing itself.

Many experiments have been devoted to studying metallurgical effects within FBC environments. These have included various alloys having a history of corrosion resistance, erosion resistance, or resistance to combined effects (19–24). Various surface treatments have also been studied and, no doubt, progress has been made (25). However, many of these experiments have been carried out in simulated combustor environments where some, but not all, of the conditions present in operating combustors have been duplicated. Also, it is probable that no two operating combustors have similar conditions, further complicating such experiments. Because of the complex set of thermal, chemical and mechanical conditions within operating FBCs, it is doubtful that response of materials in simulated environments can accurately predict which are the "best" materials for surviving the rigors of actual operating combustors. However, more credibility might reasonably be given to materials' response under actual operating conditions, and this was the basis for conducting the comprehensive study of tube sample 10–3–105 taken from the B&W tube bank that survived so well and, in fact, the basis for the entire LLNL program of which the study described in this report is but a part.

Of course, it is difficult to know how much the good response of the B&W tube bank is traceable to operational differences. That is, was the lower–chlorine–content South Hopkins coal a factor in the response obtained with the B&W tube bank? Or, were fluidization conditions or tube spacings or some other design factor, among the many differences in operating conditions, responsible for its favorable response? Some, all, or none of these variables may have been involved. But, whether they were or not, significant metallurgical differences between the tube two banks have been

identified and these differences could well have been responsible for the difference in wastage behavior - and if not wholly responsible, at least partially.

If these indications are valid, it should be practical and feasible to optimize metallurgical variables and, thereby, to produce steel tubes that possess some degree of inherent resistance to wastage in FBC environments. Since the indications were derived from actual evaporator tubes from an operating pilot plant combustor, relevance of the findings to actual combustor operation should be much greater than test results obtained in the laboratory under simulated conditions. And this should enable verification to be more readily and directly made.

There are a number of apparent metallurgical differences between the tubes of the two tube banks. The temptation is to attempt to identify differences and proceed to draw conclusions. This temptation, however, should be resisted as some of the differences observed probably are secondary effects – reflections of primary differences that are controlling. For example, an attempt to develop wastage resistance through use of steels that are merely softer than others at tube operating temperatures may not be totally effective. However, it is conceivable that deformable substrates may, of themselves, offer some benefit in being able to retain their protective scales under repetitive impact through absorbing some of the energy of impinging particulates.

The higher elevated temperature indentation hardness observed in the C–E tube is believed to be due to conditions such as restricted dislocation movement from internal oxidation or precipitation of very fine oxides along ferrite grain boundaries or within the matrix (26–28). From chemical analysis and observations of the microstructure, it would appear that such a condition does not exist in the B&W tube steel, producing the lower hardness.

When all differences are considered together, it appears that virtually all stem from a common source, and that is the steelmaking processes or production procedures used to make the steels of the two tube banks. This would not only influence chemical composition and its related effects upon inclusion content and, possibly, upon elevated temperature indentation hardness, but also upon microstructure (29–33).

The pearlite banding that is so obvious in the C–E steel may not be detrimental, per se, as such banding is normally not considered a microstructural defect. Banded steels have mechanical properties in usual testing directions that are substantially identical to those of non–banded steels. However, as was observed in these tubes, bands of pearlite tend to orient in planes parallel to the rolling or forming direction. Consequently, tensile tests of steel where the tensile axis is parallel to the banding planes show no difference due to banding.

However, banding has been observed to reduce through–thickness (short–transverse) ductility (34). This may not be a direct result of the banding itself but of segregation or some other condition that also influences banding. Since the pearlite bands observed in tubes in this study tend to lie in circular and concentric paths roughly parallel to the tube surface, it is conceivable that oxidation behavior may differ as alternating microstructures are exposed to combustor environments. More likely, however, the banding probably is simply a by–product of the steelmaking process which tends to produce segregation in an alloy essentially devoid of residual elements (as was the steel used in the C–E tube bank).

Indications are that, in production of the steel for the C–E tube bank, every attempt was made to exclude trace elements and the usual background of residuals in an effort to produce "clean" steel, free of inclusions and incidental constituents. The steel is, in fact, very clean and has a very low inclusion level. Chemical analysis shows the steel is a simple alloy of iron, carbon, manganese and silicon, and little else. The steel of the B&W tube bank, on the other hand, has residuals of a good many other elements, typical of usual scrap charges. While its composition certainly is not substandard and would conform to applicable ASTM and other compositional specifications, it is evident that no particular steps were taken to exclude residual trace elements. The treatment given to such a steel to assure ingot soundness and hot–malleability, probably through ladle additions before pouring, would include an addition of aluminum and possibly a rare earth metal addition (lanthanum, for example) to assist in desulfurizing.

It is not surprising, therefore, that the behavior of these two steels at elevated temperature under the oxidizing and sulfurizing conditions of a coal combustion environment was different. This is, of course, evident in the fact that one steel was susceptible to wastage while the other was not. More specifically, however, a principal difference (and one probably influencing wastage response) was in the thickness and appearance of the scales that formed on these two steels. This difference also persisted in the laboratory oxidation tests conducted in the simple atmosphere of heated still air.

Clues to the reason for differences in scales formed on the two steels may be found in the microanalytical studies conducted of cross sections in the vicinity of the scale/substrate interface. An outstanding difference was chromium enrichment in the scale near the interface, noted in the B&W steel, as well as an enrichment there of nickel, silicon, manganese, probably molybdenum (although confirmation of the presence of this element was obscured by other spectral lines) and, possibly, aluminum. Many of these elements are known to affect scale growth and are well–established principal alloying elements in boiler tube steels (35). Although these elements are added to such steels in considerably greater amounts, the degree of enrichment that was estimated from high resolution EDS analyses certainly could account for the oxidation–resistance observed in the B&W steel.

In the C–E steel, the levels of these elements were low; consequently, no enrichment of them was observed at the scale/substrate interface. Only silicon concentration was observed at the interface of the C–E steel. It is interesting to note that although the C–E steel itself had a higher manganese content (0.70% vs 0.54% for the B&W steel), the manganese concentration observed at the interface of the B&W steel was much greater than that at the interface of the C–E steel. Similarly, the silicon concentration in the B&W steel also was higher. It is possible that the silicon buildup noted at interfaces of both steels may have been contamination from polishing media used in preparing the samples. This would be particularly likely in the B&W sample where the scale was fractured, creating a crevice for polishing–media to lodge. Nevertheless, as discussed earlier, silicon is a constituent of all surface scales and is probably derived from bed materials.

Although the reasons are not fully understood at this time, there appears to be a difference between the two steels in the rate of concentration of elements at or along the scale/substrate interface, with the B&W steel showing consistently higher levels of all observed elements (noted, primarily, in laboratory oxidation tests conducted on both steels at the same time where combustor complications were absent). Differences in scale growth in the oxidation tests were consistent with the buildup of residual elements at or near the scale/substrate interface (36–42).

While not measured during this study, there may be other differences in properties of scales formed on the two steels. Growth rate apparently is different, as observed in the samples exposed to oxidation tests. And the scales differ in appearance, as well. However, there may also be differences in their elevated temperature hardness, friability, or resistance to exfoliation by impacting bed material, and in differences in adhesion to the substrate. Such differences would not be unexpected, considering the extent of differences that have already been observed between them.

As noted earlier, scale that formed on the B&W steel had a thin, different-appearing, layer at or near the steel substrate. This layer was observed to be fractured (pulled away) from the substrate, but remained intact with it. As mentioned before, this fracture possibly occurred during sample preparation due to shrinkage of the mounting medium. However, this layer evidently is relatively brittle and easily fractured. Since the elemental concentrations observed in this steel were at or just below this fractured (pebbly appearing) layer, it is conceivable that any scale exfoliation that may occur on the B&W steel would be confined to loss of the outer layer of oxide, leaving the inner and elementally–enriched layer firmly attached to the steel substrate. If so, it would offer a case of resistant material to protect the steel, possibly not only from mechanical impacts but also from metal loss due to excessive rates of oxidation, as might occur if exfoliated scale exposed bare, unprotected and unalloyed carbon steel (as probably occurs in the C–E steel).

While the effects of alloying elements upon the oxidation resistance of iron that have been observed in the tubing steels studied in this program are consistent with known principles, it is difficult to attempt to explain protection mechanisms on the basis of observations made on only a few samples of steel. However, some possibilities are apparent. It is known, for example, that additions of elements like silicon, chromium and aluminum to iron can influence its oxidation behavior (43). It apparently does this through accumulation of a layer of oxide of the added element/s at the interface of the iron substrate, as formation of such a layer produces a notable change in the oxidation–time curve. Evidently, the presence of this layer interferes with diffusion of iron from the metal substrate into the oxide scale. Such "insulation" would, therefore, tend to diminish oxidation rate of the metal (44–45).

This is observed in the two steels oxidized in the laboratory furnace (Figure 22). In the absence of residual trace elements, a relatively thick oxide layer formed in the 100–hour test. In the other steel, the oxide layer was not only thinner (suggesting a slower rate of formation), but there also was a much different appearing interface layer adjacent to the steel substrate. And EDS traverses across this layer showed a buildup of a number of elements, including chromium, silicon, nickel and manganese.

These observations, when reviewed in the context of response of these steels in the combustor, would suggest at first glance that low–alloy steels (e.g. 2 $\frac{1}{4}$% Cr–1% Mo steel) would offer a high degree of resistance to FBC wastage. However, this has not consistently been the experience although Cr–Mo steels have shown an improvement (46). This was observed in the previous study of tubes from Series 2 experiments at Grimethorpe, mentioned before. Tubes from tube bank C–2 (2 $\frac{1}{4}$% Mo steel) had significantly less wastage than the carbon steel tubes of tube bank C, but wastage still occurred. Apparently, there are several characteristics of tubing steels that are involved in their wastage response, and oxidation rate may simply be one of them. The effects on FBC tubing wastage of several co–present alloying elements, and within a steel produced by an unknown set of process steps, are not easily understood.

At first, it may be difficult to understand how a steel having trace amounts of several alloying elements (like steel 10–3–105 of this study) could offer superior response in FBC environments to a low–alloy Cr–Mo steel having a few percent of alloying constituents (47). It is conceivable, however that, despite their chromium and molybdenum contents, these steels may lack other ingredients (such as, e.g. aluminum, silicon, manganese) essential for developing not only the necessary degree of oxidation resistance, but possibly also the ability to form a spinel or spinel–hematite or magnetite sub–layers to impart the necessary abrasion resistance to the constant impinging and scouring of bed materials. From observations made in these studies, it would appear that both of these characteristics are essential in achieving long life for in–bed evaporator tubing.

8.3 Future Work and Recommendations

This study has suggested a number of possibilities for imparting wastage resistance to carbon steel for in–bed evaporator tubes. As appealing as these possibilities are, they must be regarded as strictly initial indications based upon limited data until further confirming work has been done. Such work should include preparation, preferably on a controlled experimental basis, of steel compositions representing a number of steelmaking alternatives and following the leads uncovered in this program. Systematic variations in elemental residuals, added one–at–a–time and in various combinations, should be made to an otherwise identical basic composition of steel of constant carbon content.

The resulting ingots should be forged and worked sufficiently to reproduce as nearly as possible the condition and microstructures of commercially–processed tubing. Samples of the forged steels would be chemically analyzed and evaluated metallographically and their results compared. If the materials are as intended, samples could be subjected to laboratory oxidation tests to evaluate scale–forming behavior and the morphology and composition of sub–layers that formed at and near the interface. If these tests on experimentally–produced steels confirm indications observed in actual combustor tubes, additional quantities of the materials should be worked into lengths of tubing suitable for installation in an operating combustor where effects of metallurgical variables might be confirmed under actual FBC conditions.

9.0 CONCLUSIONS

1. As identified in a previous study of tubes from Series 2 experiments at the Grimethorpe PFBC facility in the U.K., metal wastage of these tubes also appears to occur through exfoliation of protective oxide scale. Scale loss is probably caused by impingement and abrasion by bed materials.

2. There is no evidence that chemical effects, other than oxidation of exposed or exfoliated steel surfaces, are responsible for or contribute to the wastage process.

3. Significant metallurgical differences have been observed between tube metal of wastage–susceptible and wastage–resistant tube banks. The wastage–resistant tube, because of higher levels of microalloying residuals, forms an alloy–enriched layer at the scale/substrate interface that is believed to serve as a protective shield in minimizing the detrimental effects of mechanical impacts of impinging bed particulates and in providing an oxidation resistant layer on the carbon steel substrate.

4. The protective layer that forms on the wastage–resistant tubes is probably a function of the steelmaking process used in production of the tubing ingot stock and is thought to be responsible, to a large degree, for the superior response of the tubing of the initial TVA tube bank.

10.0 REFERENCES

1. Witherell, C. E. and Meisenheimer, R. G., *Tubing Wastage in Fluidized-Bed Coal Combustors – Examinations of Tubing from Test Series 2, NCB (IEA Grimethorpe) Ltd.-Facility*, UCRL-97569, Lawrence Livermore National Laboratory, Livermore, CA 94550 (October 30, 1987). See also *Proceedings of Workshop on Wastage of In-Bed Surfaces in Fluidized-Bed Combustors*, Volume III, Argonne National Laboratory, Argonne, IL (November 2–6, 1987) 5.11.

2. Witherell, C. E. and Meisenheimer, R.6., *Tubing Wastage in Fluidized Bed Coal Combustors – Test Series 2, NCB (IEA Grimethorpe) Ltd.*, UCRL-21039, Lawrence Livermore National Laboratory, Livermore, CA 94550 (January 8, 1988).

3. Wheeldon, John, letter of July 7, 1987 to C. E. Witherell.

4. Ibid.

5. Wheeldon, John, letter of August 28, 1987 to C. E. Witherell.

6. Witherell, C. E. and Meisenheimer, R. G., Reference 2, op. cit. p. 5–6.

7. Witherell, C. E. and Meisenheimer, R. G., References 1 and 2, op. cit.

8. Cooke, M. J. and Rogers, E. A., "Investigations of Fireside Corrosion in Fluidized Combustor Systems," *Fluidized Combustion*, Proceedings of an International Conference held at Imperial College, London, U.K. (16–17 September 1975) Institute of Fuel Symposium Series No. 1. B6-1 – B6-10.

9. Raask, E., *Wear.* 13 (1969) 301.

10. Clauss, F. J., *Engineer's Guide to High Temperature Materials,* Addison-Wesley Publishing Co. (1969).

11. Evans, U. R., *The Corrosion and Oxidation of Metals, Scientific Principles and Practical Applications*, Second Edition, Edward Arnold, London (1960). 27–9

12. Wright, I. G., Nagarajan, V., and Stringer, J., "Observations on the Role of Oxide Scales in High-Temperature Erosion-Corrosion of Alloys," *Oxidation of Metals*, 25, Nos. 3/4 (1986) 175–99.

13. Stringer, J. and Wright, I. G., "Materials Issues in Fluidized Bed Combustion," *Journal of Materials for Energy Systems*, 8, No. 3 (December 1986) 319–31.

14. Levy, E. K. and Bayat, F., "Effect of Type of Bubble/Tube Interaction on Rate of Erosion," *Proceedings of Workshop on Wastage of In-Bed Surfaces in Fluidized Bed Combustors*, Argonne National Laboratory, Argonne, IL, (November 2–6, 1987), 4.4

15. Elliott, P., Tyreman, C. J., and Prescott, R., "High Temperature Corrosion by Halogens", *Journal of Metals* (July 1985) 20–23.

16. Potter, E. C. and Nancarrow, P. C., "Corrosion Caused by Coal Combustion", *Proceedings of Conference on Australian Coal Science* 2, Volume 1, Wahroona, Australia, Australian Institute of Energy (1986) 93–7.

17. Nateson, K., "Metal Wastage Analysis of Carbon Steel Tubes from TVA 20 MW AFBC" *Proceedings of Workshop on Wastage of In–Bed Surfaces in Fluidized–Bed Combustors*, Argonne National Laboratory, Argonne, IL (November 2–6, 1987) 5.10.

18. Witherell, C. E. and Meisenheimer, R. G., Reference 1, op. cit.

19. Wright, I. G., Nagarajan, V., and Merz, W. E., *Erosion–Corrosion of Metals and Alloys at High Temperatures*, Report No. CS–3504 (June 1984), Electric Power Research Institute, Palo Alto, CA 94304.

20. Wilhelmsson, P., "Hot Corrosion of Heat–Resistant Alloys in Simulated Fluidized Bed Combustion Environment," Chapter 19 of *Corrosion Resistant Materials for Coal Conversion Systems*, (Meadowcroft, D. B. and Manning, M. I., eds.), Applied Science Publishers, Ltd., New York, NY (1983) 389–404.

21. Nazemi, A. H., Smith, E. P., Madsen, M. M., Malone, G. A., and Davis, R. D., *Analysis of Metal Wastage in Coal–Fired Fluidized Bed Combustors*, Final Report DOE/MC/21351–2019, The MITRE Corp., McLean, VA 22120 (December 1985) Table 3–3, p 3–6.

22. Nazemi, A. H., Madsen, M. M., and Malone, G. A., *Characterization and Analysis of Metal Wastage in Coal–Fired Fluidized–Bed Combustors,* Interim Report (August 1985), The MITRE Corp., McLean, VA 22102.

23. Nagarajan, V., Wright, I. G., and Smith, R. D., "Morphology of Corrosion of Advanced Heat Exchanger Materials in Simulated FBC Deposits." *Proceedings, Corrosion–Erosion–Wear of Materials in Emerging Fossil Energy Systems,* Berkeley, CA (January 27–29, 1982), National Association of Corrosion Engineers, Houston, TX 77084, 493–510.

24. Nagarajan, V., Rocazella, M. A., Wright, I. G., and Smith, R. D., "The Morphology of Sulfidation Corrosion in the Oscillating Oxygen/Sulfur Partial Pressure Environments Observed In Fluidized Bed Coal Combustors," Chapter 18 of *Corrosion Resistant Materials for Coal Conversion Systems*, (Meadowcroft, D. B. and Manning, M. I., eds.), Applied Science Publishers, Ltd., New York, NY (1983) 371–88.

25. Canonico, D. A., "Fluidized Bed Combustor Wastage 20 MW AFB Remedies – Coatings," *Proceedings of Workshop on Wastage of In–Bed Surfaces in Fluidized–Bed Combustors*, Argonne National Laboratory, Argonne, IL (November 2–6, 1987) 6.3

26. Yearian, H. J., Randell, E. C., and Longo, T. A., "The Structure of Oxide Scales on Chromium Steels," *Corrosion*, 12 (October 1956) 235–67.

27. Hauffe, K., *Oxidation of Metals*, Plenum Press, New York, NY (1965) 335–64.

28. Swisher, J. H., "Internal Oxidation," Chapter 12 of *Oxidation of Metals and Alloys*, American Society for Metals, Metals Park, OH (1971) 235–67.

29. Holappa, L. E. K., "Ladle Injection Metallurgy," *International Metals Reviews*, Vol. 27, No. 2 (1982) 53–76.

30. *Microalloying 75 Proceedings*, October 1–3, 1975, Washington, DC.

31. Honeycombe, R. W. K., "Some Aspects of Microalloying," *Transactions of the Japan Institute of Metals*, Vol. 24, No. 4 (1983) 177-89.

32. Lange, K. W., "Thermodynamics and Kinetic Aspects of Secondary Steelmaking Processes," *International Materials Reviews*, Vol. 33, No. 2 (1988) 53–89.

33. Smith, G. V., *Elevated Temperature Static Properties of Wrought Carbon Steel*, ASTM Special Technical Publication 503 (STP 503), American Society for Testing and Materials, Philadelphia, PA 19103 (1972).

34. Samuels, L. E., *Optical Microscopy of Carbon Steels*, American Society for Metals, Metals Park, OH 44073, (1980) 127–31.

35. Evans, U. R., Reference 11, op. cit. 63.

36. Wood, G. C. and Medford, M. A., "The Examination of Oxide Scales on Iron–Chromium Alloys by X–Ray Scanning Microanalysis," *Journal of the Iron and Steel Institute*, (June 1961) 142–8.

37. Caplan, D. and Cohen, M., "High Temperature Oxidation of Chromium–Nickel Steels," *Corrosion*, 15 (March 1959) 141t–146t.

38. Yearian, H. J., Randell, E. C., and Longo, T. A., Reference 26, op. cit. 515t–525t.

39. Lai, D., Borg, R. J., Brobers, M. J., Mackenzie, J. D., and Birchenall, C. E., "Oxidation of Iron–Chromium Alloys at 750–1025C," *Corrosion*, 17 (July 1961) 357t–364t.

40. Kofstad, P., *High Temperature Oxidation of Metals*, John Wiley & Sons, Inc. (1966) 264–99.

41. Douglass, D. L., "Exfoliation and the Mechanical Behavior of Scales," Chapter 8 in *Oxidation of Metals and Alloys*, American Society for Metals, Metals Park, OH (1971) 137–56.

42. Birchenall, C. E., "Oxidation of Alloys," Chapter 10 in *Oxidation of Metals and Alloys*, American Society for Metals, Metals Park, OH (1971) 177–234.

43. Evans, U. R., Reference 11, op. cit. 60–9.

44. Kubaschewski, O., and Hopkins, B. E., *Oxidation of Metals and Alloys*, Second Edition, Academic Press Inc., New York, NY (1962) 103–37.

45. Hauffe, K., Reference 27, op. cit. 267–314.

46. Carls, E. L., Wheeldon, J. M., Minchener, A. J. and Brooks, S., "Review of Wastage of IEA Grimethorpe Tube Bundles," *Proceedings of Workshop on Wastage of In-Bed Surfaces in Fluidized-Bed Combustors*, Argonne National Laboratory, Argonne, IL (November 2–6, 1987) 5.9.

47. Stringer, J. and Wright, I. G., "Erosion/Corrosion in FBC Boilers," *Proceedings of Workshop on Wastage of In-Bed Surfaces in Fluidized-Bed Combustors*, Argonne National Laboratory, Argonne, IL (November 2–6, 1987) 1.1.

TABLE 1

Operational Information on TVA
AFBC Tubing Samples Studied

Tube Identification	27–A–1	27–A–4	8–1	10–3–105
Combustor Row	1	4	1	3
Tube Bank Manufacturer(1)	C–E	C–E	C–E	B&W
Tubing O.D. (mm)	53.9	53.9	53.9	50.8
Tubing Wall Thickness (mm)	6.3	6.3	6.3	5.8(2)
Combustor Exposure (hrs)	4,735(3)	4,735(3)	3,904(4)	13,625(5)
Wastage (mm/1000 hrs)	0.3	0.3	0.30	0.03
Nominal Bed Temperature (C)	850	850	850	850
Tube Temperature (C)	370	370	370	370
Bed Fluidizing Velocity (m/sec)	2.4	2.4	2.4	2.4
Mean Bed Particle Size (μm)	600–800	600–800	600–800	600–800
Bed Material (limestone ash, wt %)	75–92	75–92	75–92	75–92

(1) C–E: Combustion Engineering (second tube bank)
B&W: Babcock and Wilcox (original tube bank)

(2) Spirally–fluted inside bore

(3) Comprising 9 test periods (1986–1987):
Test periods 1–6 (1986): 3,904 hrs, "Pyro" Coal, Cl content = 0.30 wt %
Test period 7 (1987): 213 hrs, "Warrior" Coal, Cl content = 0.05 wt %
Test period 8 (1987): 276 hrs, "Warrior" Coal, Cl content = 0.05 wt %
Test period 9 (1987): 342 hrs, "Pyro" Coal, Cl content = 0.30 wt %

(4) Comprising 6 test periods (1986): 3,904 hrs, "Pyro" coal, Cl content = 0.30 wt %
(Note: This was the same exposure as test periods 1–6 of above footnote)

(5) "South Hopkins" coal, Cl content = 0.02 wt %, used for entire coal burning period of 13,625 hrs

TABLE 2

Chemical Compositions of Tubing Samples*

Element	Chemical Analysis (wt.%)	
	Sample No. 27–A–4	Sample No. 10–3–105
Iron	Balance	Balance
Aluminum	0.007	0.06
Boron	<0.0005	<0.0005
Carbon	0.24	0.25
Cerium	<0.005	<0.005
Chromium	0.01	0.12
Columbium	<0.005	<0.005
Copper	0.008	0.07
Lanthanum	<0.005	0.010
Magnesium	<0.002	<0.002
Manganese	0.70	0.54
Molybdenum	<0.005	0.03
Nickel	0.01	0.05
Nitrogen	0.005	0.009
Oxygen	0.002	0.004
Phosphorus	0.014	0.014
Silicon	0.18	0.14
Sulfur	0.006	0.022
Titanium	<0.005	<0.005
Tungsten	<0.03	<0.03
Vanadium	<0.005	<0.005
Zirconium	<0.005	<0.005

* Samples taken from tubing mid–wall to assure a region chemically unaffected by scale or combustor environment.

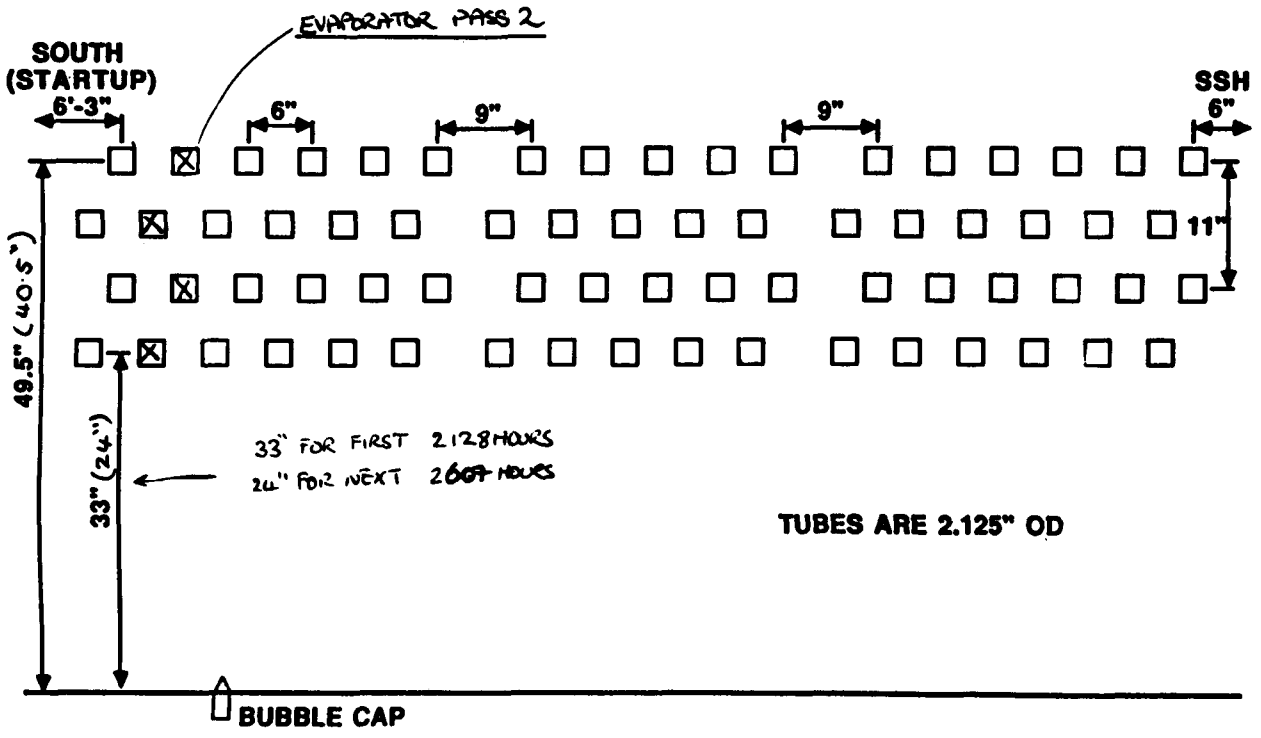

FIGURE 1-A

Locations of Tubes Examined by LLNL from Second (C-E) Tube Bank
of TVA 20 Megawatt AFBC Pilot Plant

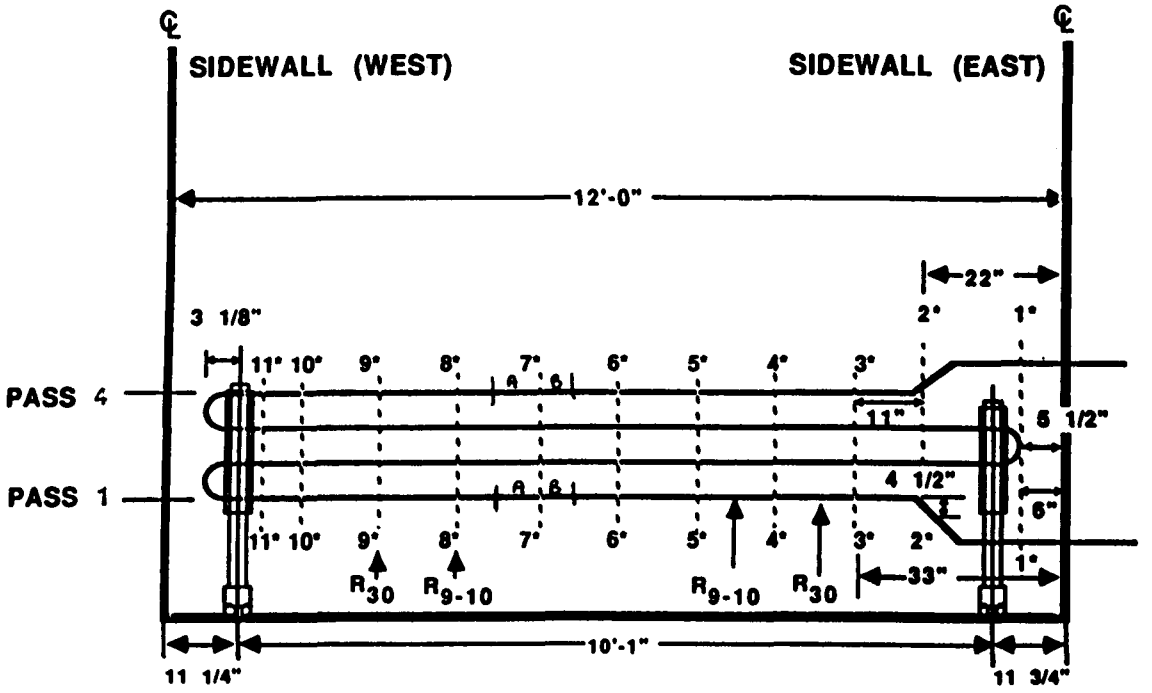

° LOCATIONS

FIGURE 1-B

Locations of Tube Sections (7A) Examined by LLNL
from Second (C-E) Tube Bank of TVA 20 Megawatt AFBC Pilot Plant

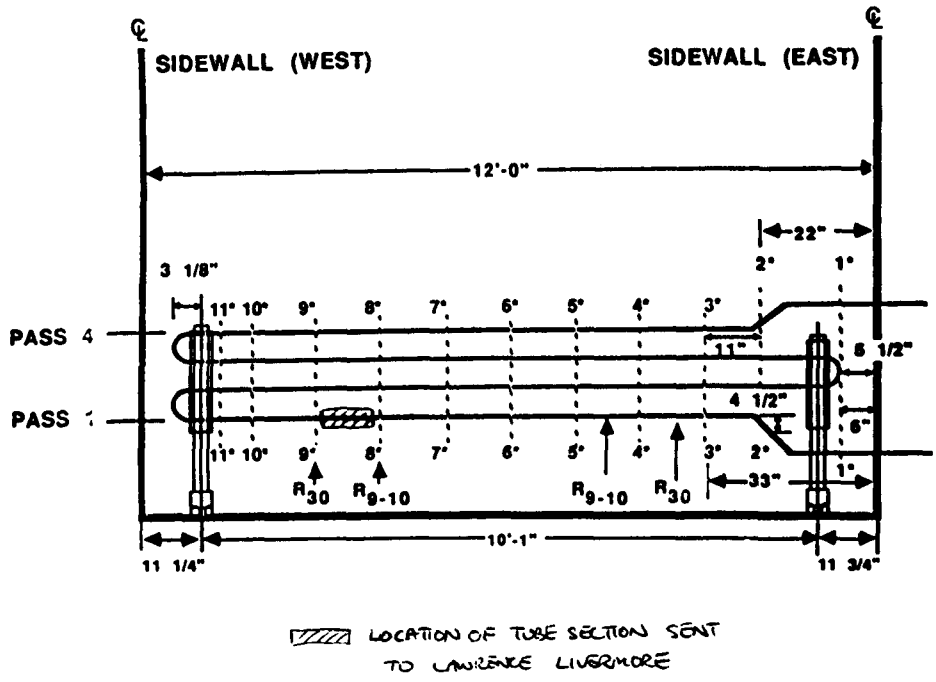

Side Elevation

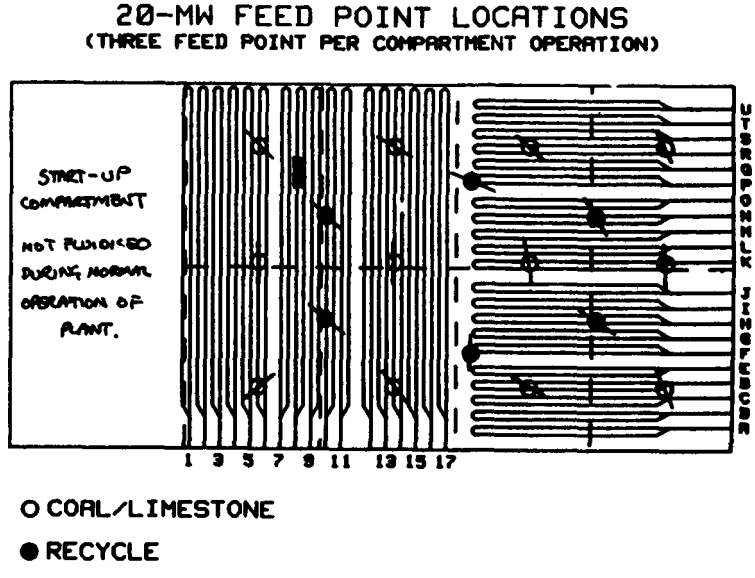

Plan View

FIGURE 2

Location of Tube Section (8-1) Examined by LLNL
from Second (C-E) Tube Bank of TVA 20 Megawatt AFBC Pilot Plant

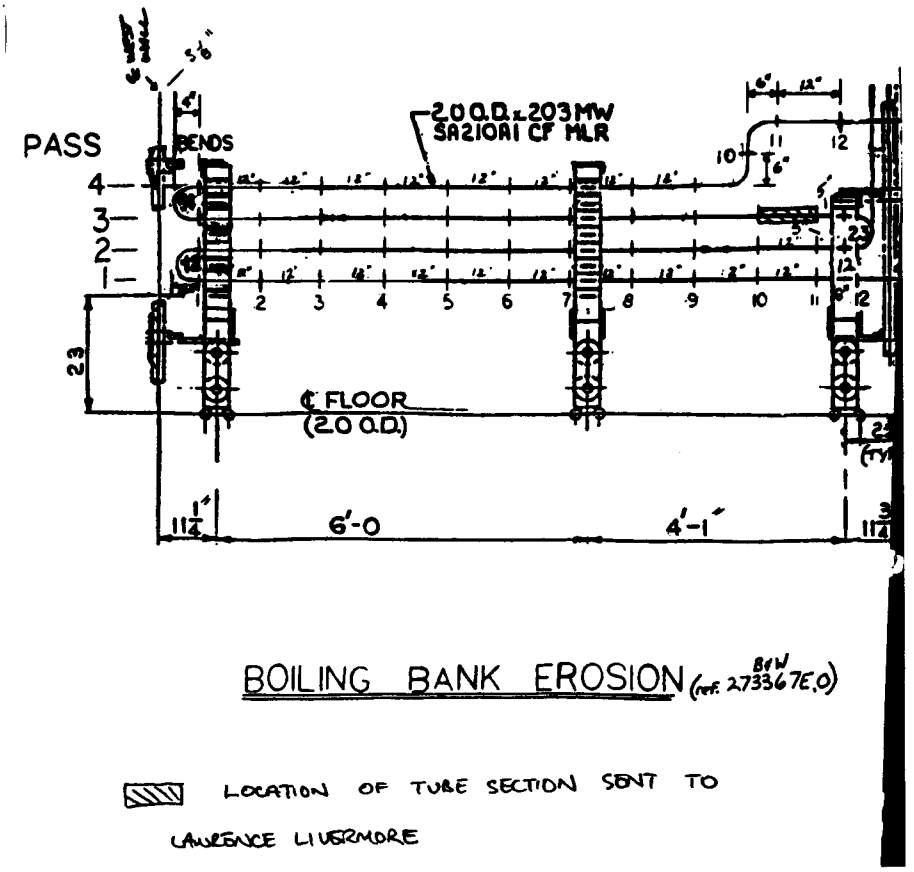

Side Elevation

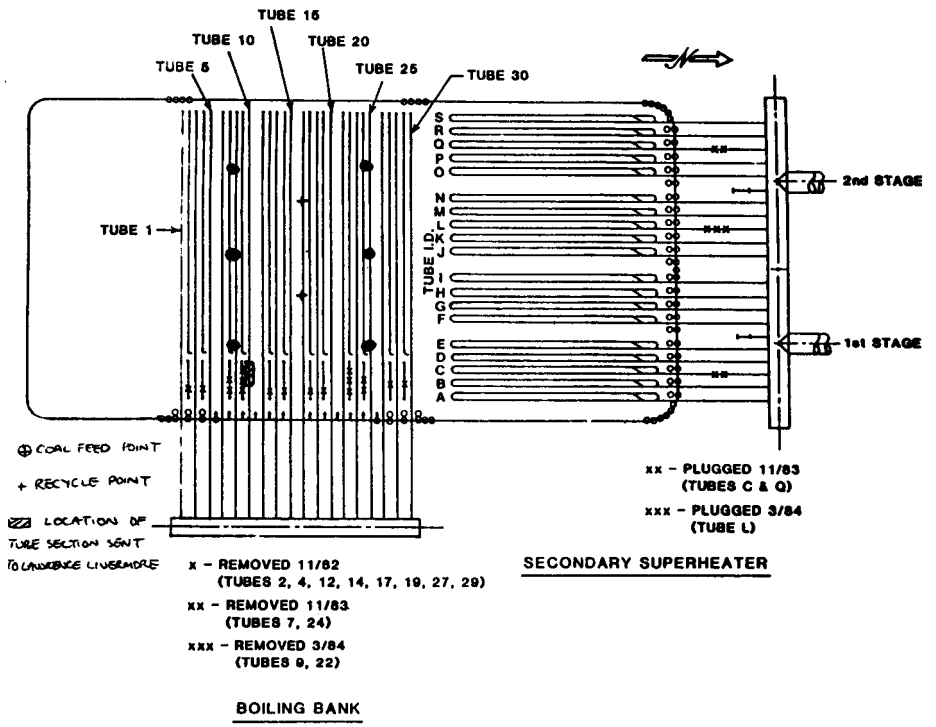

Plan View

FIGURE 3

Location of Tube Section (10-3-105) Examined by LLNL
from First (B&W) Tube Bank of TVA 20 Megawatt AFBC Pilot Plant

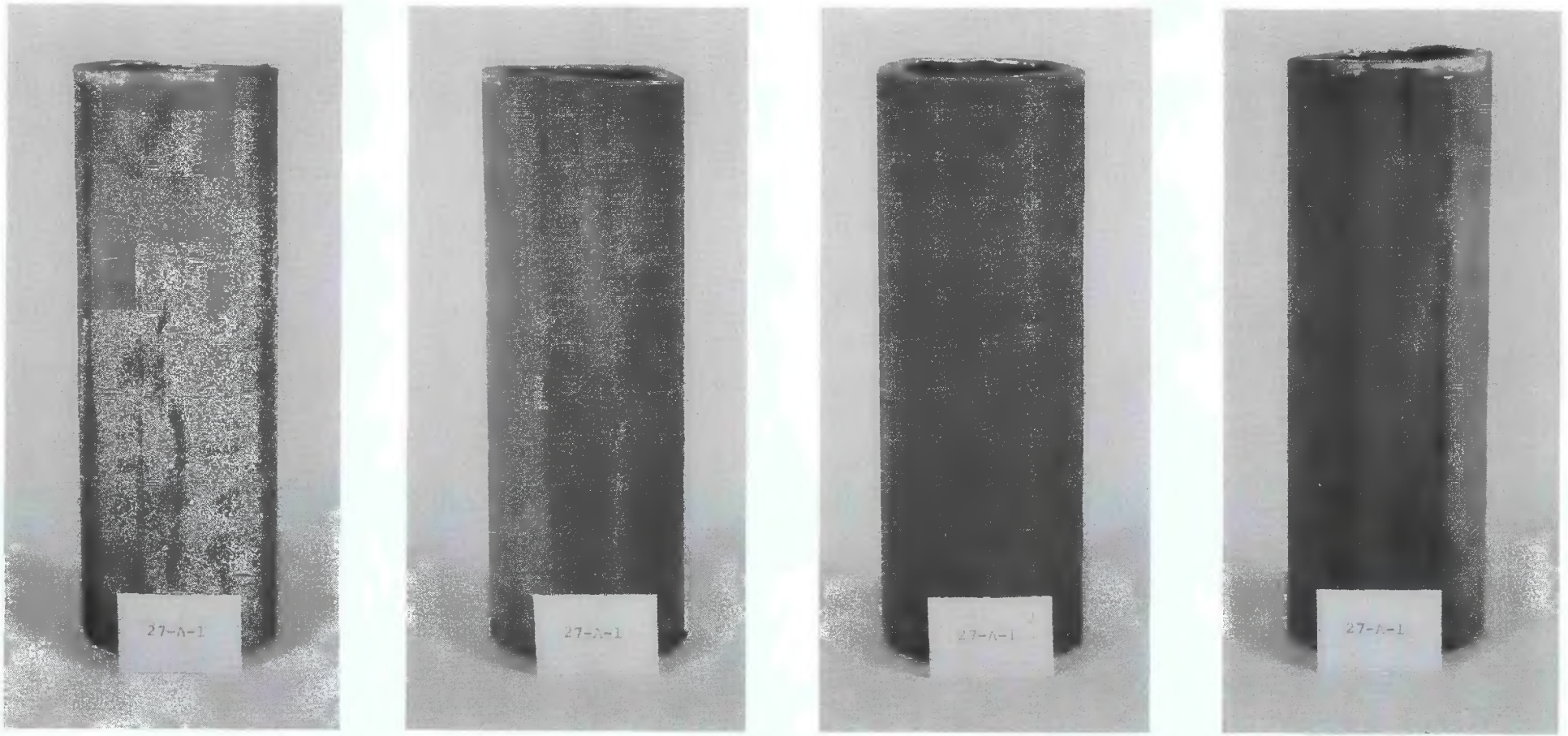

FIGURE 4-A

External Appearance of Tubing Sample 27-A-1

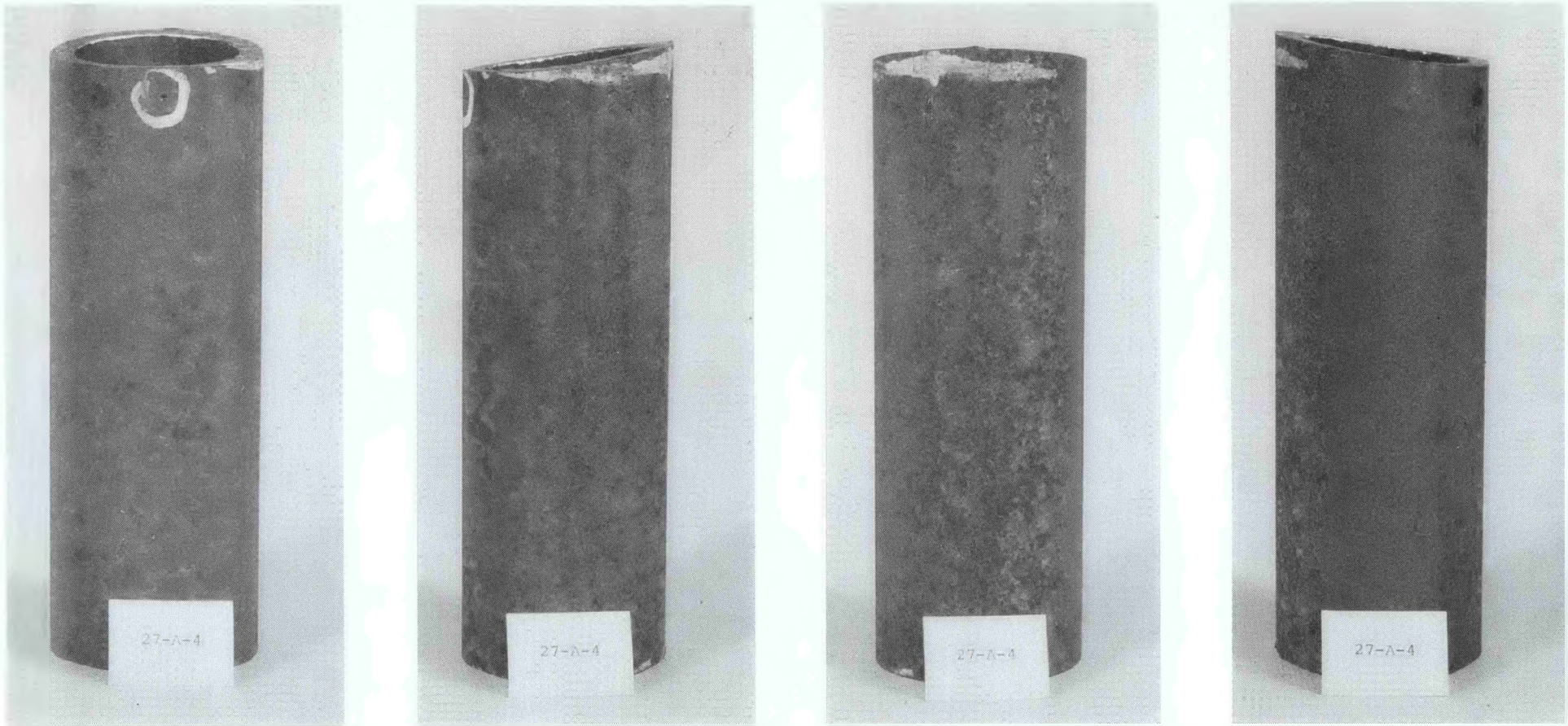

FIGURE 4-B

External Appearance of Tubing Sample 27-A-4

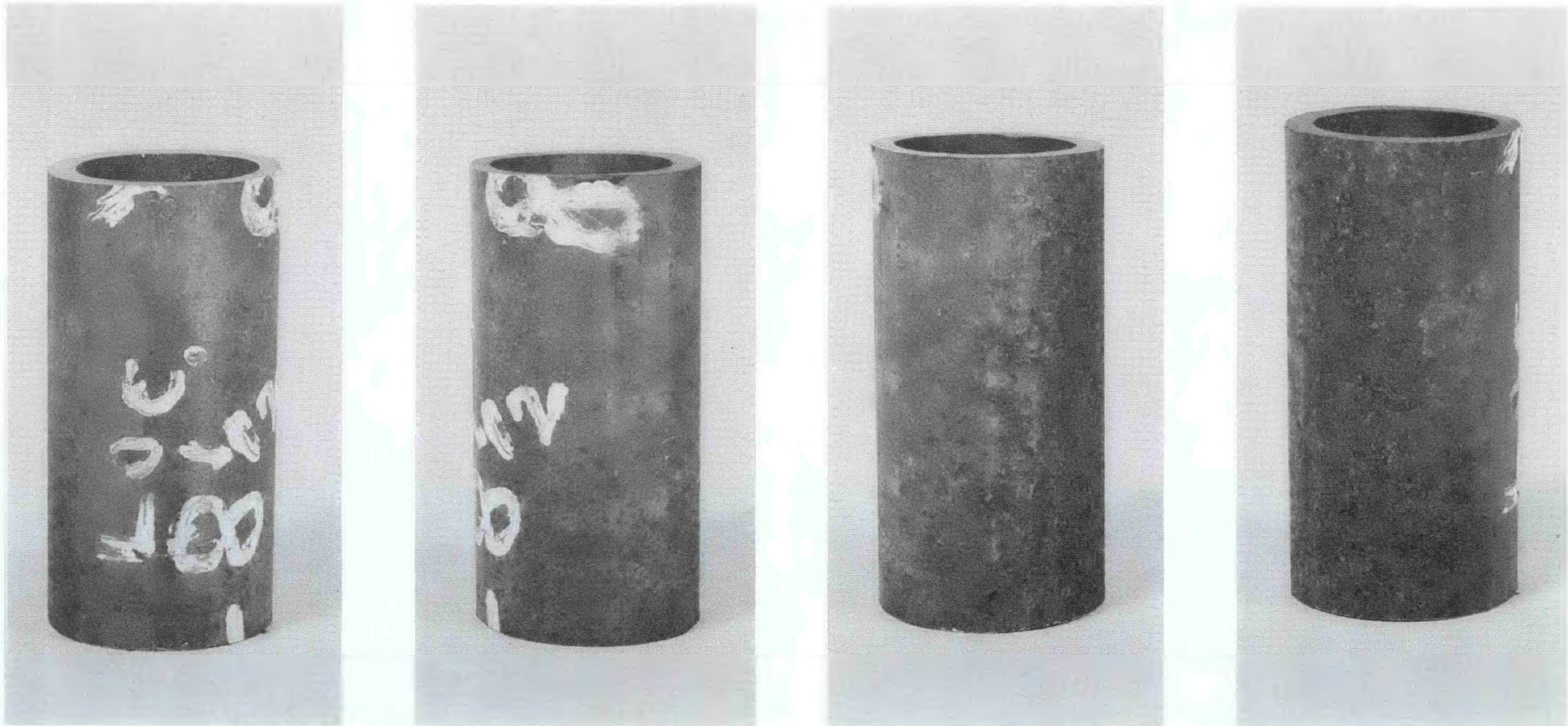

FIGURE 4-C

External Appearance of Tubing Sample 8-1

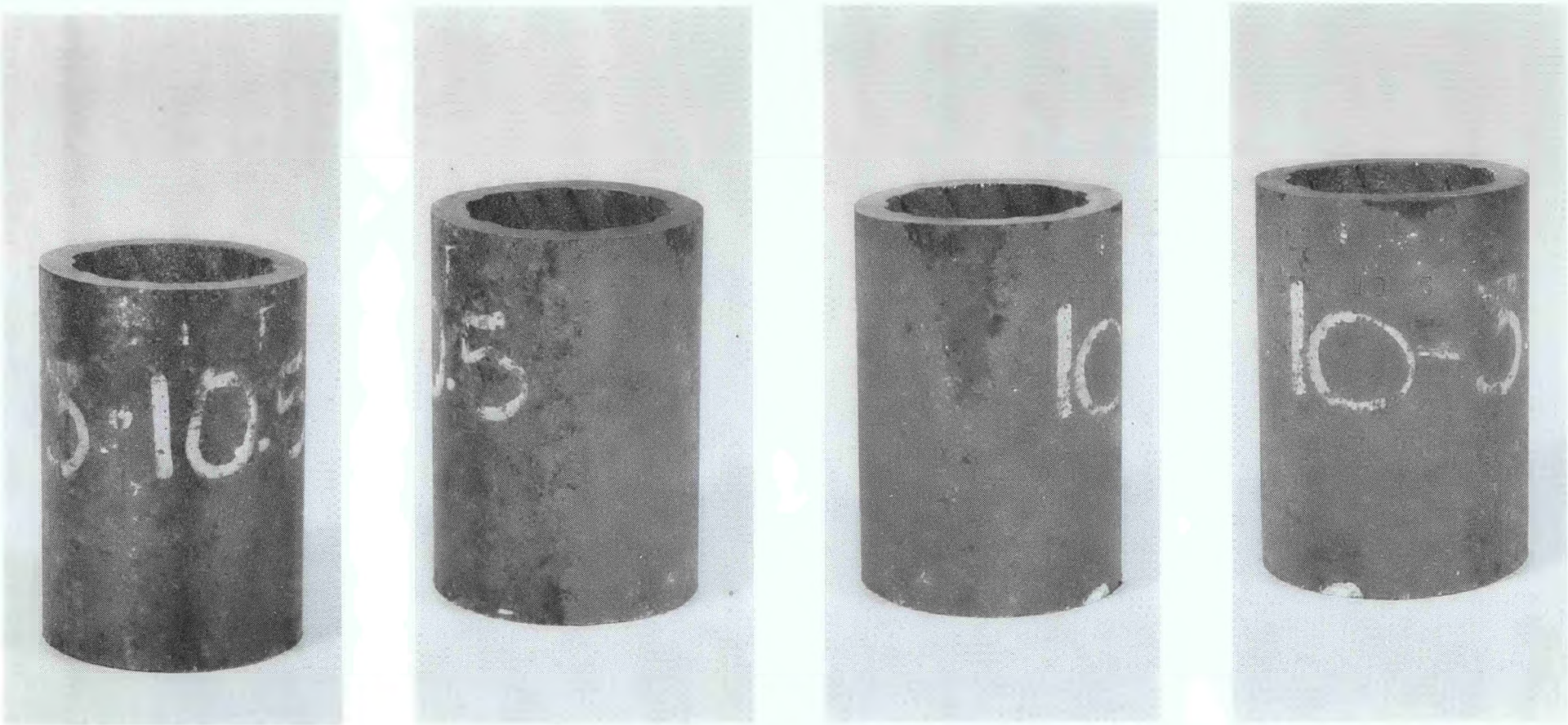

FIGURE 4-D

External Appearance of Tubing Sample 10-3-105

Sample 27-A-4 Sample 27-A-1

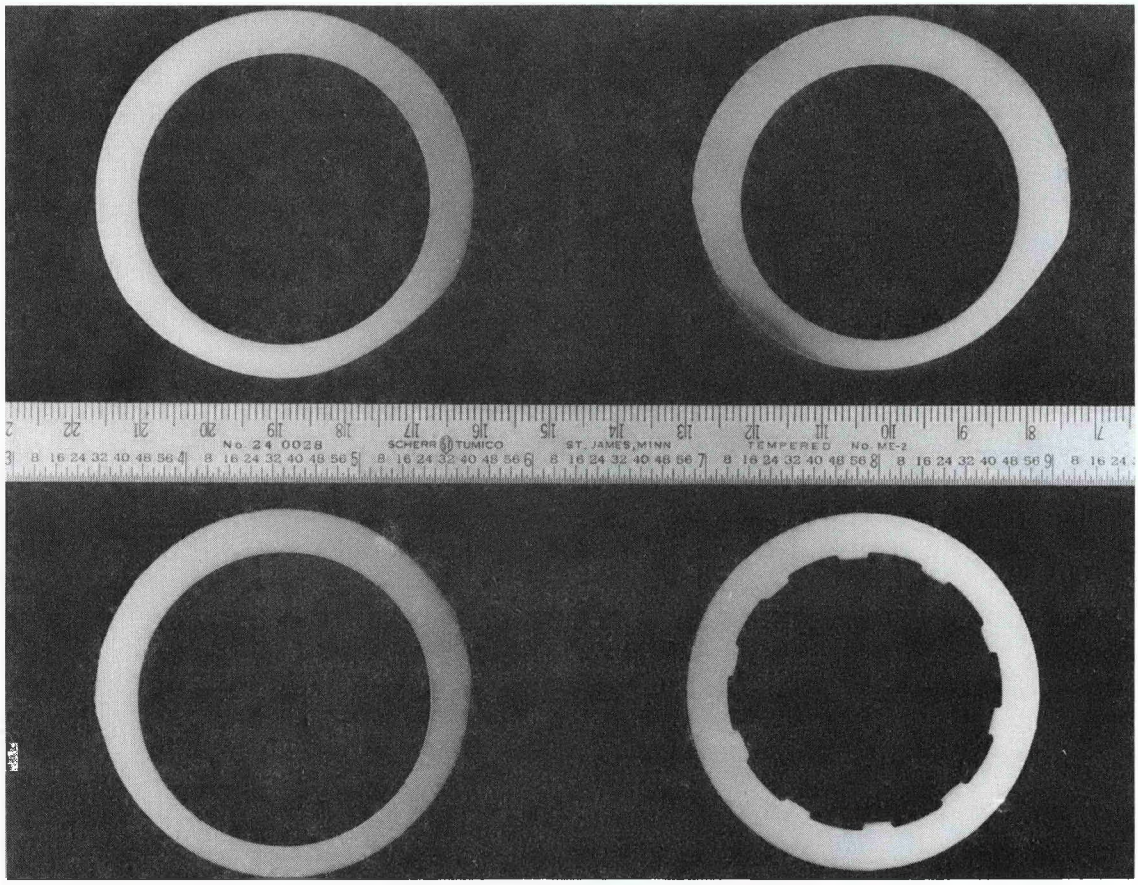

Sample 8-1 Sample 10-3-105

FIGURE 5

Cross Sections of the Four Tubing Samples Examined by LLNL

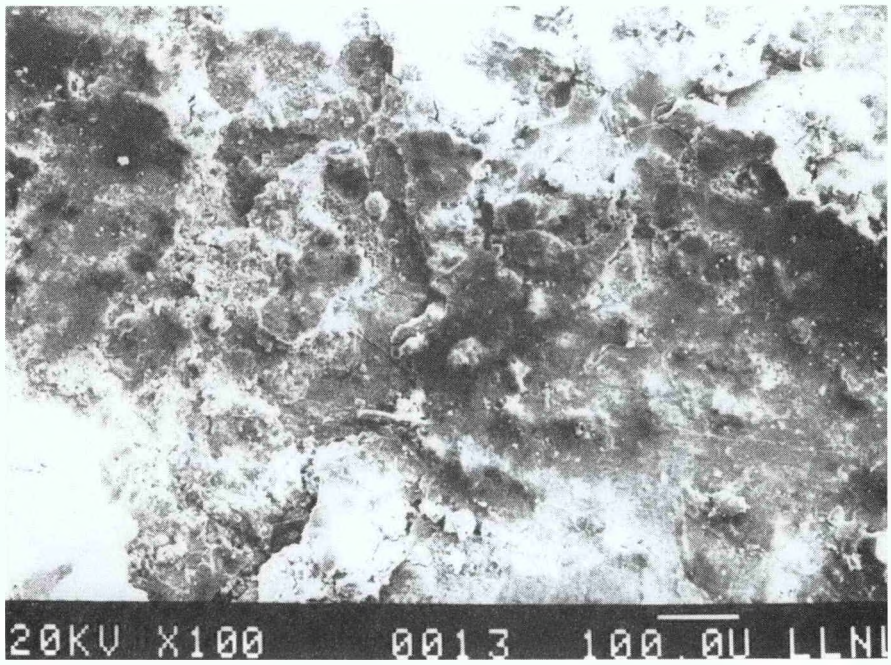

Non-Wasted Region

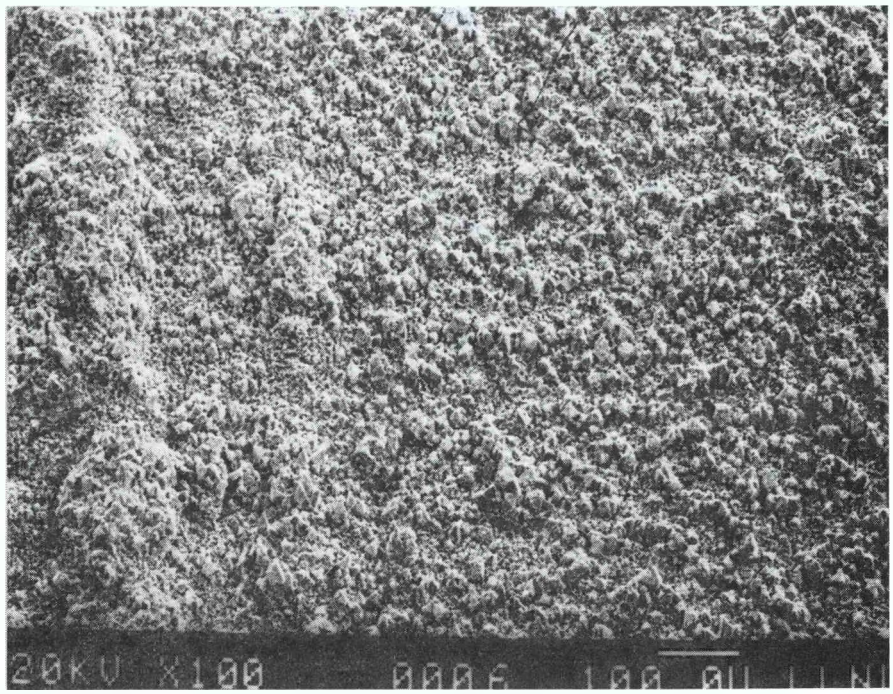

Wasted Region

FIGURE 6

Typical Appearance of Fireside Surface of Tubing Sample 27-A-1
(SEM Photomicrographs)

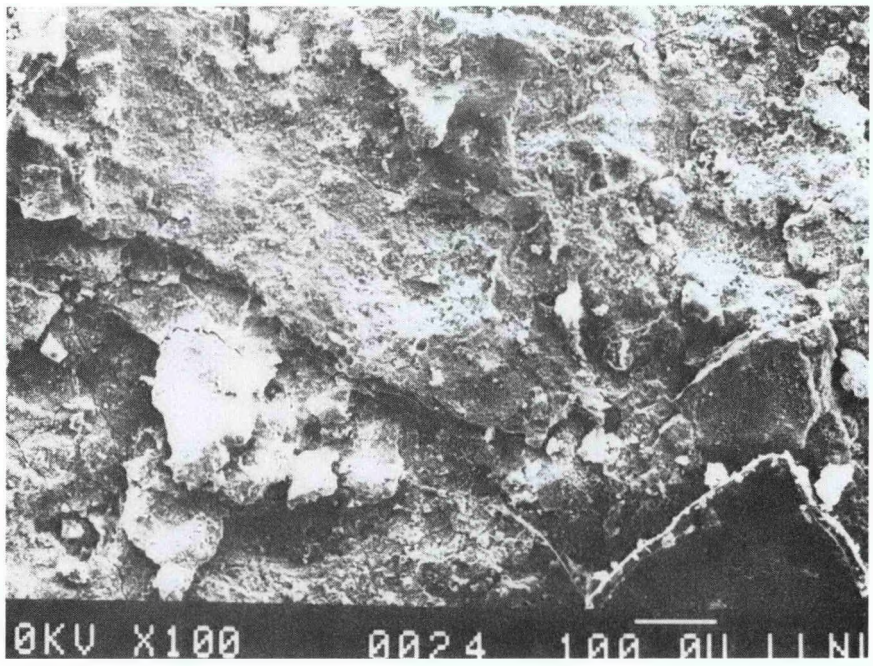

Non-Wasted Region

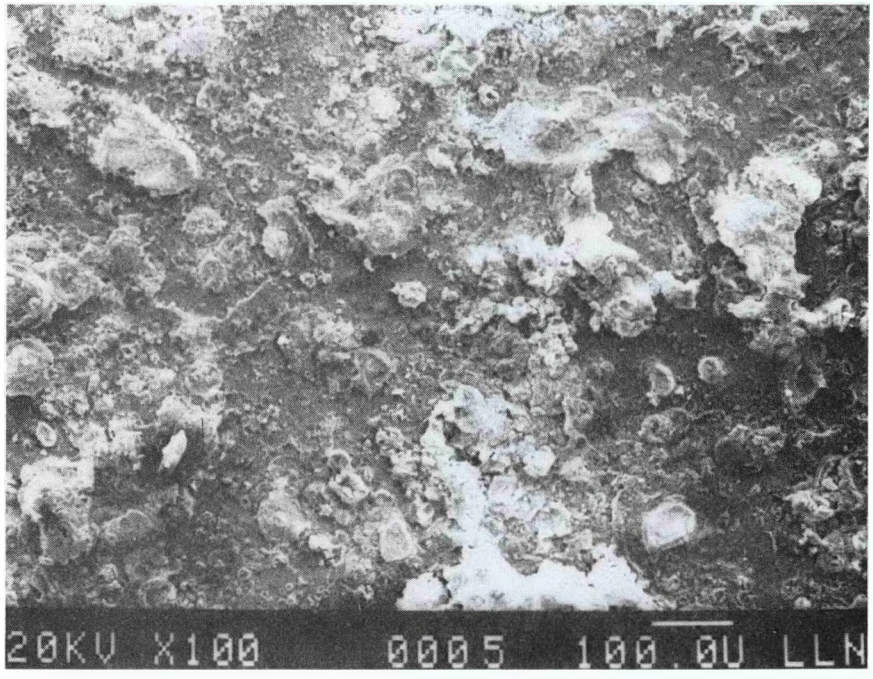

Wasted Region

FIGURE 7

Typical Appearance of Fireside Surface of Tubing Sample 27-A-4
(SEM Photomicrographs)

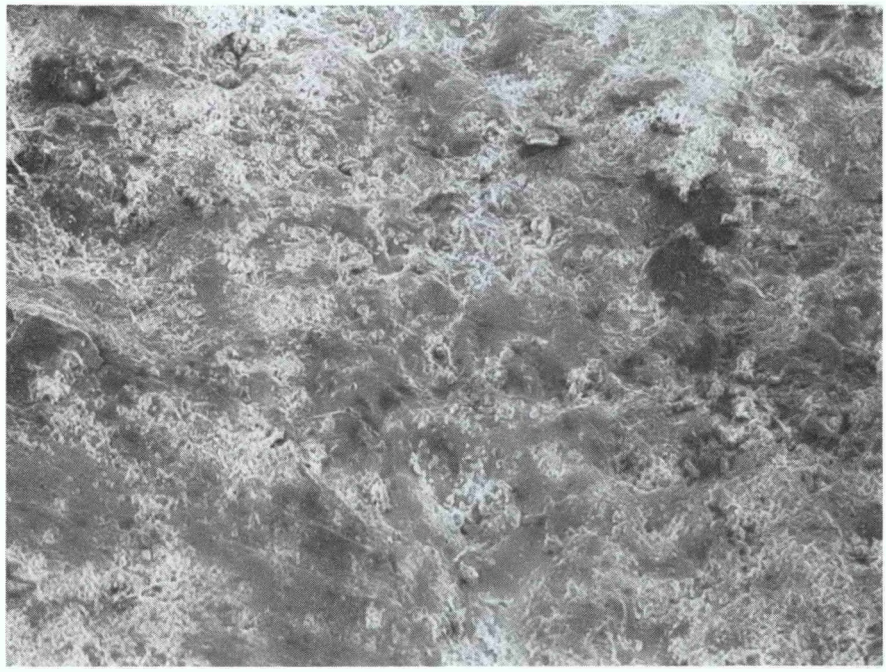

Non-Wasted Region (Magnification: about 100x)

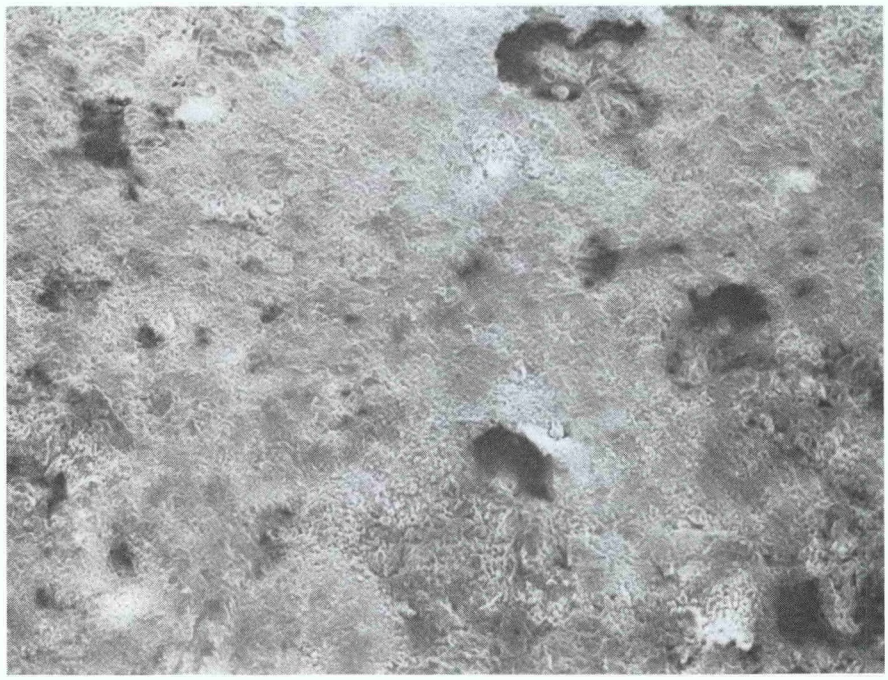

Wasted Region (Magnification: about 100x)

FIGURE 8

Typical Appearance of Fireside Surface of Tubing Sample 8-1
(SEM Photomicrographs)

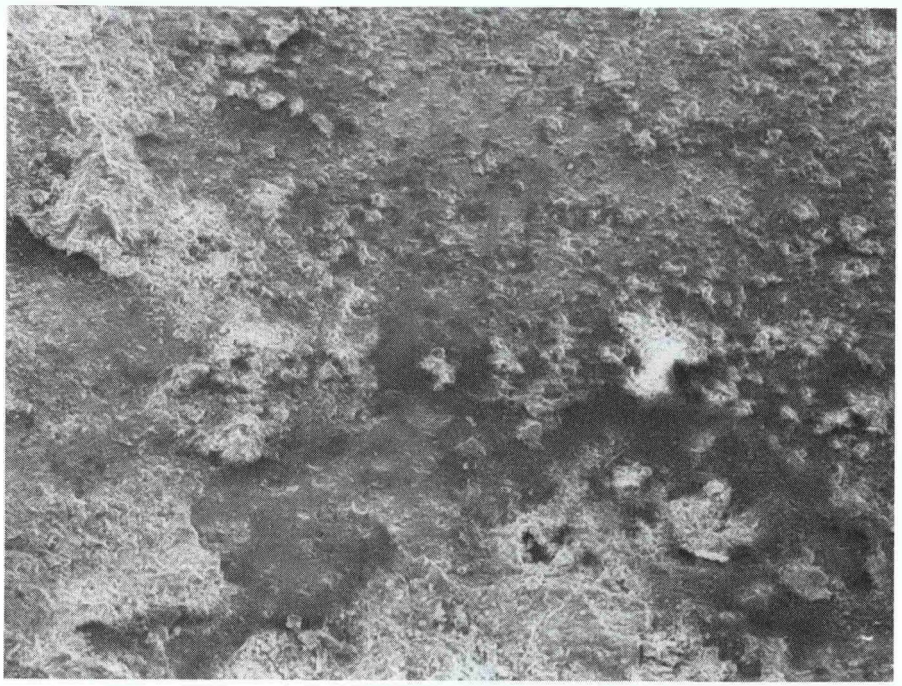

Magnification: about 100x

FIGURE 9

Typical Appearance of Fireside Surface of Tubing Sample 10-3-105
(SEM Photomicrograph)

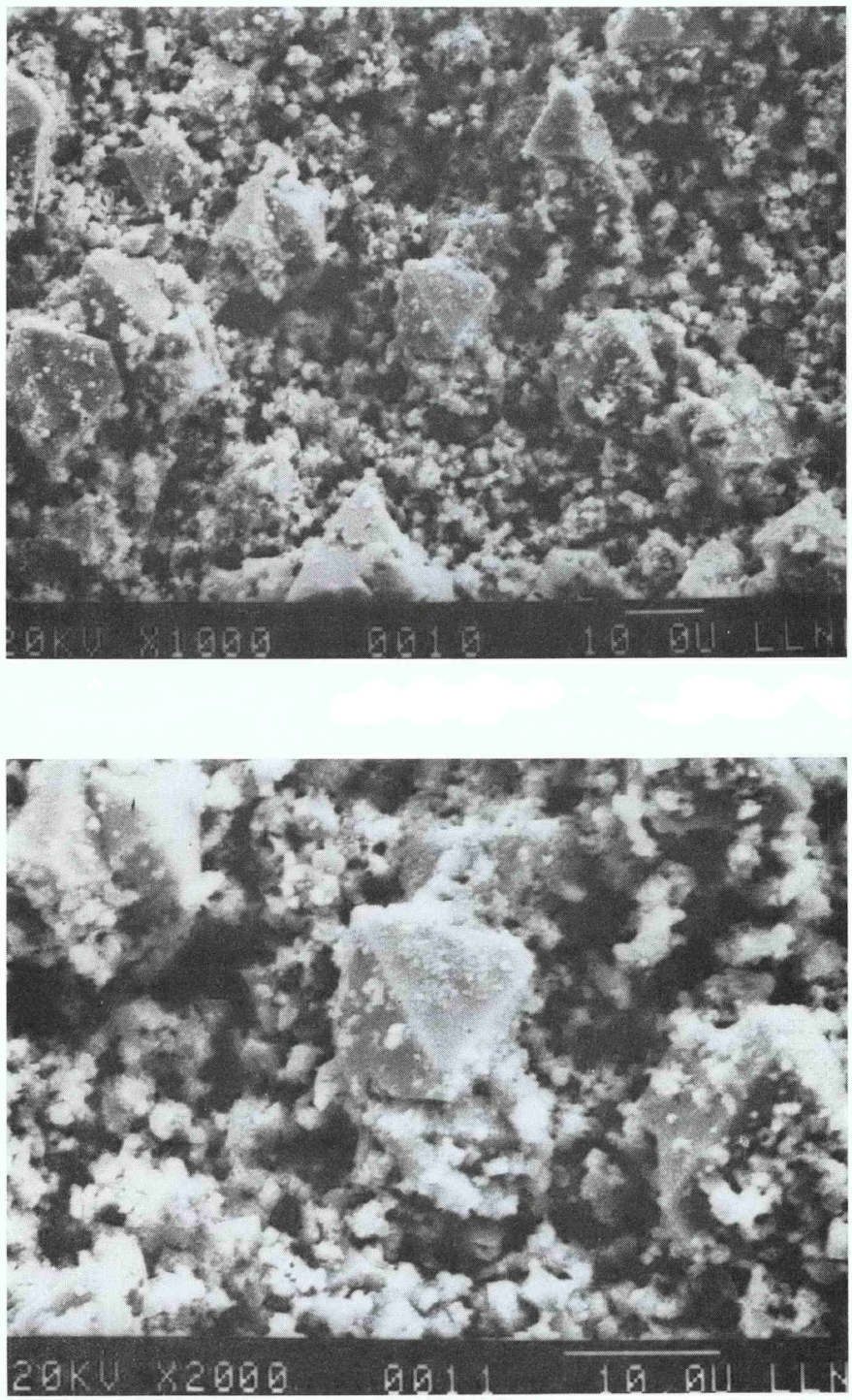

FIGURE 10

Wasted Surface of Tubing Sample 27-A-1
(SEM Photomicrographs)

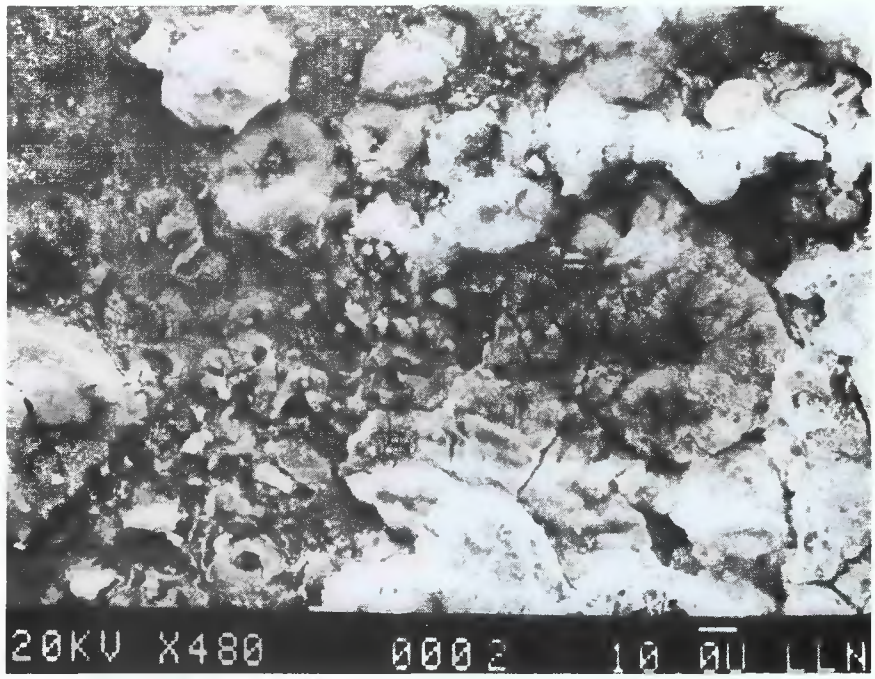

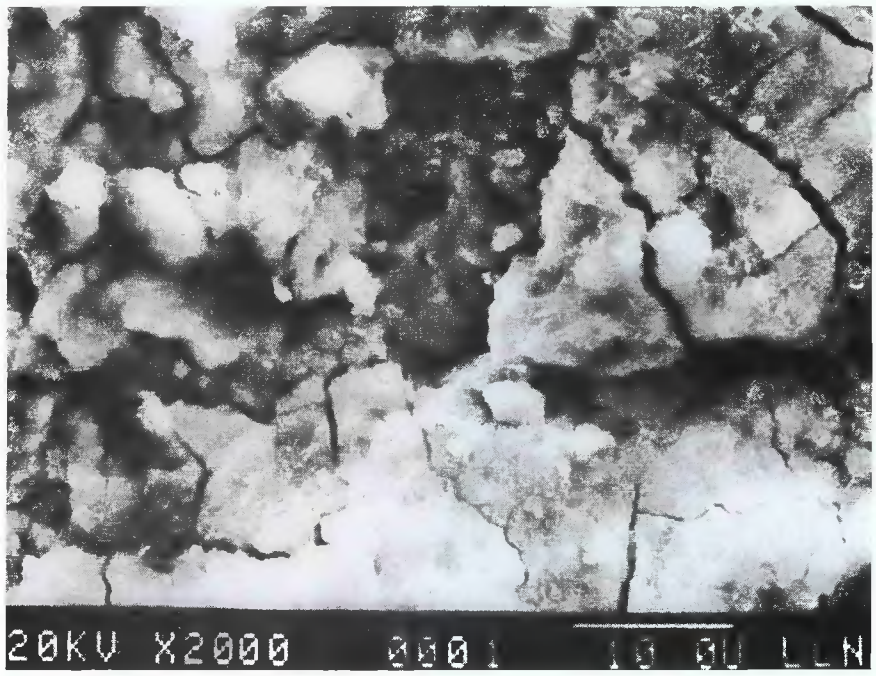

FIGURE 11

Wasted Surface of Tubing Sample 27-A-4
(SEM Photomicrographs)

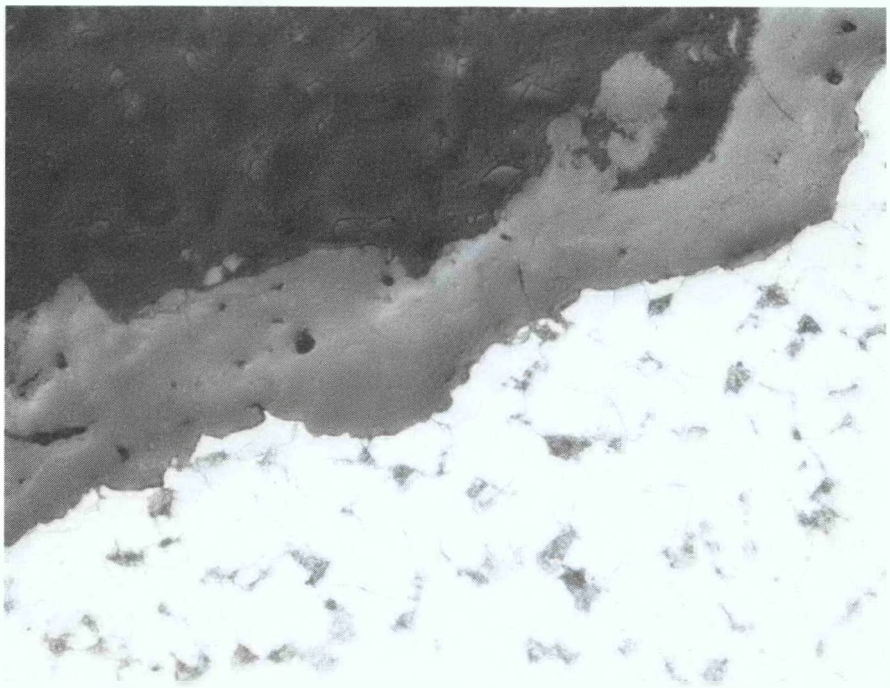

Etchant: 2% Nital Non-Wasted Region 400x

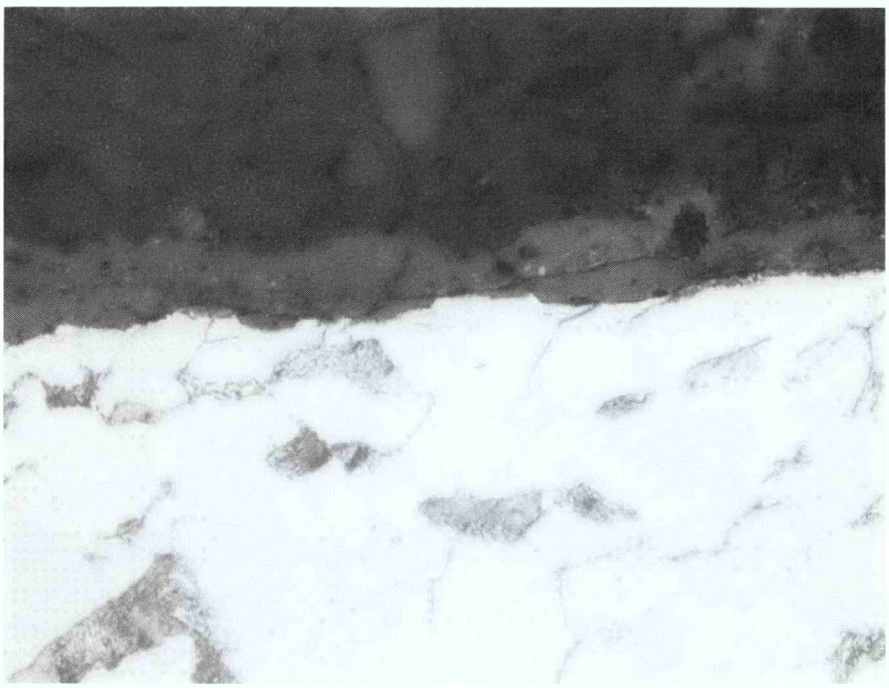

Etchant: 2% Nital Wasted Region 1,000x

FIGURE 12

Cross Sections of Tubing Sample 8-1 Showing Appearance of Surface Scale in Wasted and Non-Wasted Regions (Optical Photomicrographs - **Note different magnifications**)

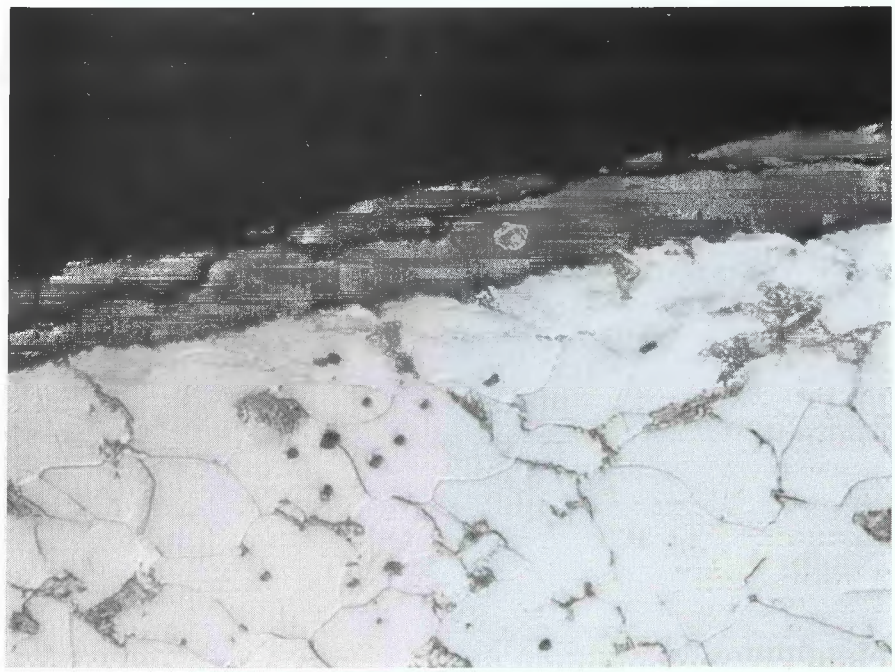

Etchant: 2% Nital 1,000x

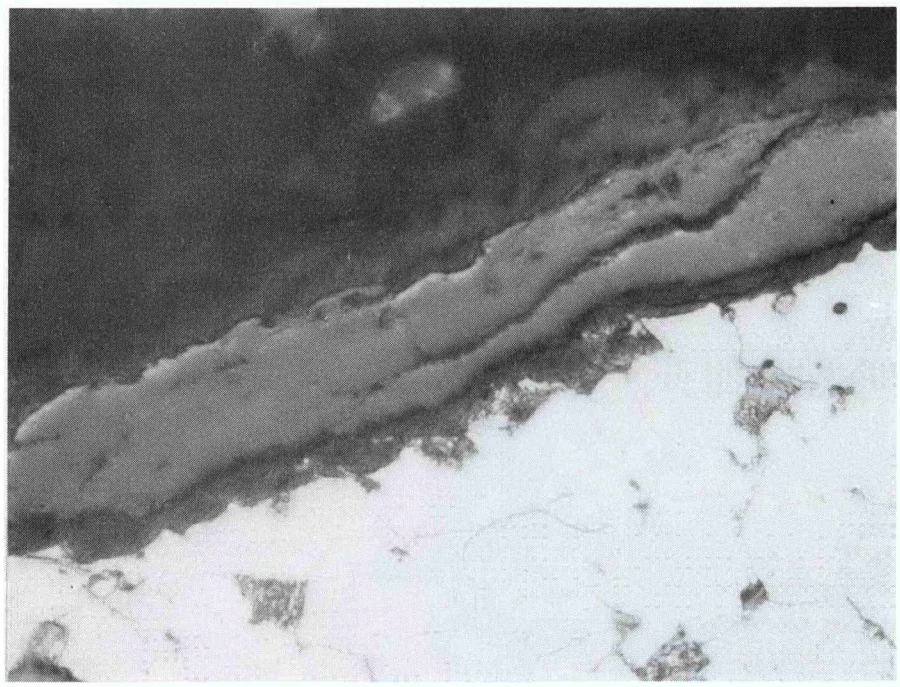

Etchant: 2% Nital 1,000x

FIGURE 13

Cross Sections of Tubing Sample 10-3-105 Showing Appearance of Surface Scale in Two Regions (Optical Photomicrographs)

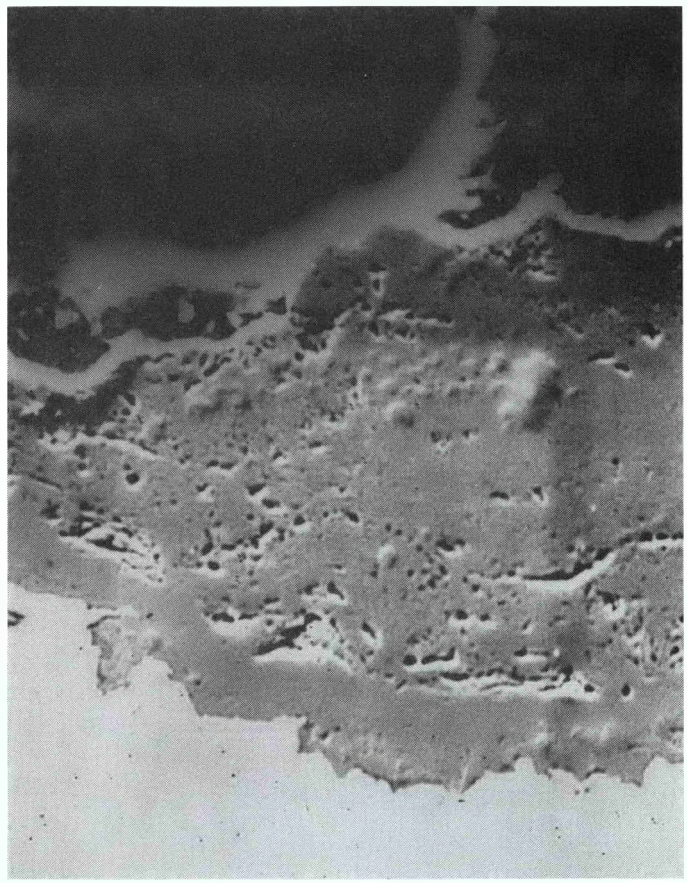

FIGURE 14-A

Cross Section of Non-Wasted Region of Tubing Sample 27-A-4
(SEM Secondary Electron Image of Area Used for XRF Maps of Figure 14-B)

Sulfur

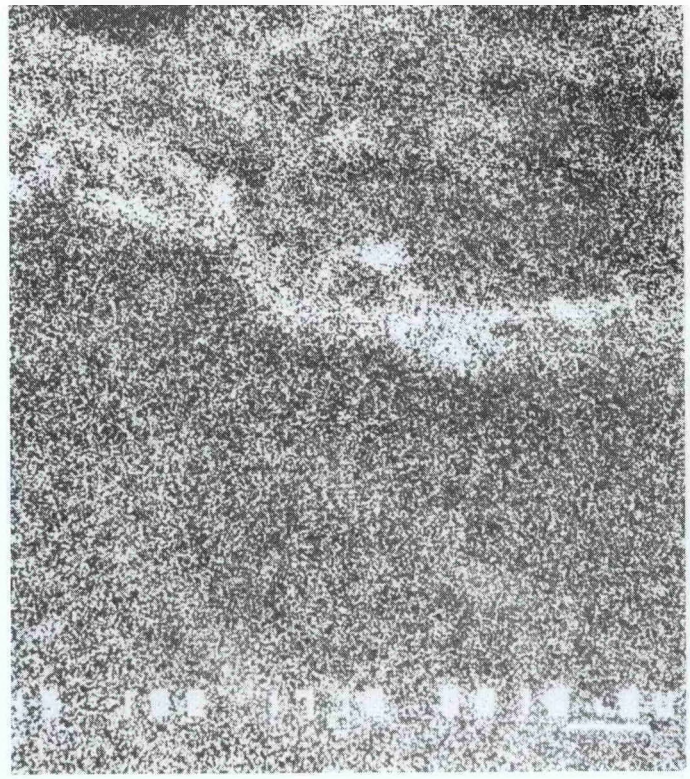

Potassium

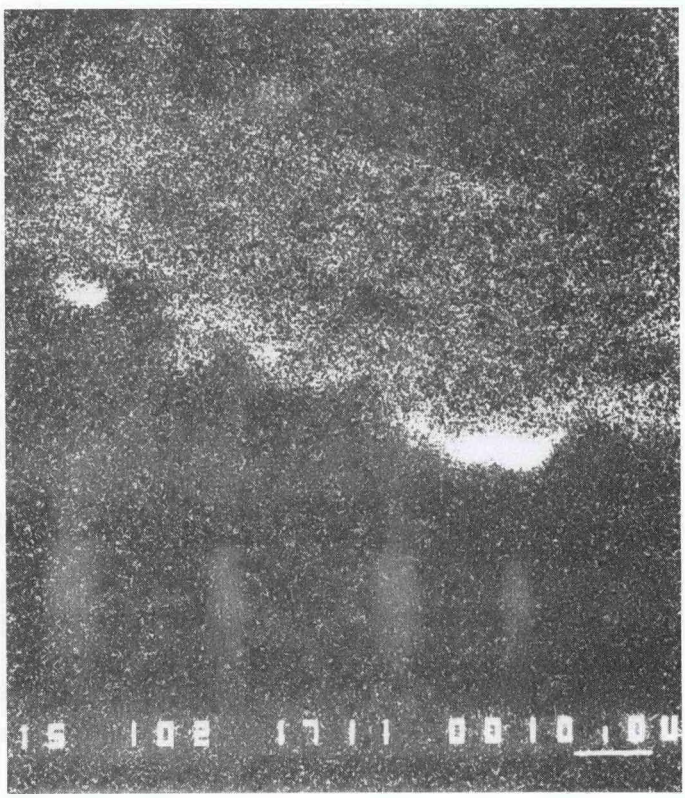

Chlorine

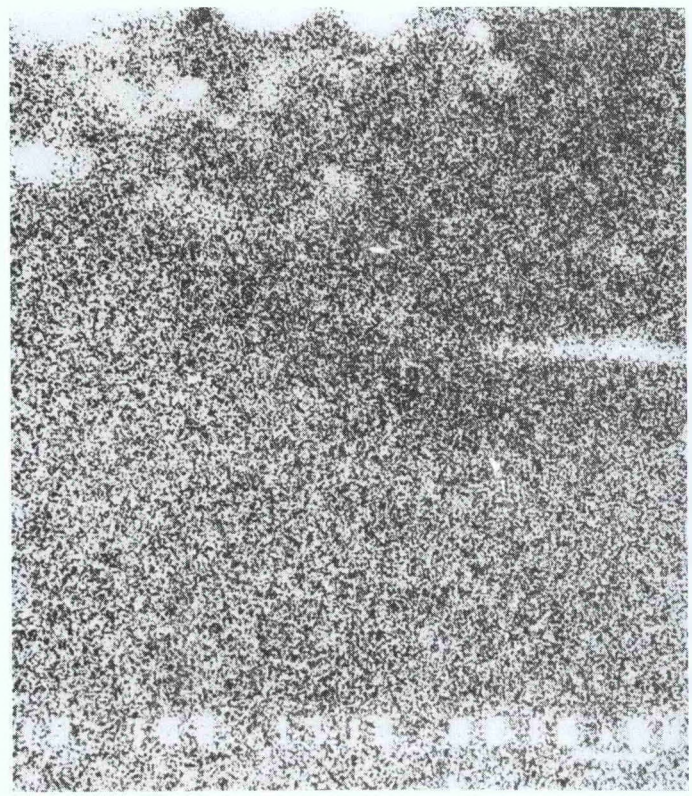

Calcium

FIGURE 14-B

XRF Element Maps of Cross Section of Non-Wasted Region
of Tubing Sample 27-A-4

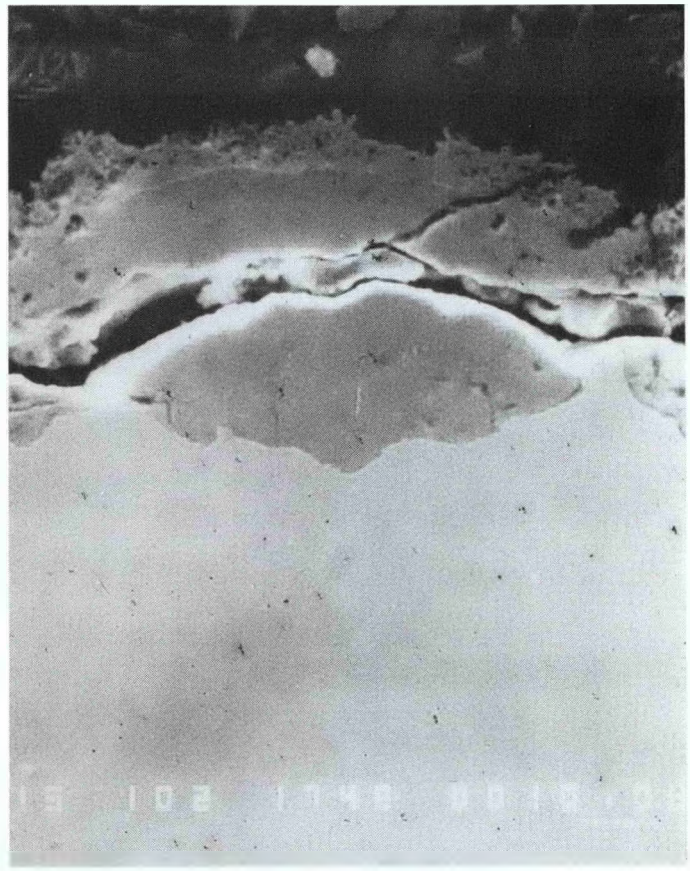

FIGURE 15-A

Cross Section of Wasted Region of Tubing Sample 27-A-4
(SEM Secondary Electron Image of Area Used for XRF Maps of Figure 15-B)

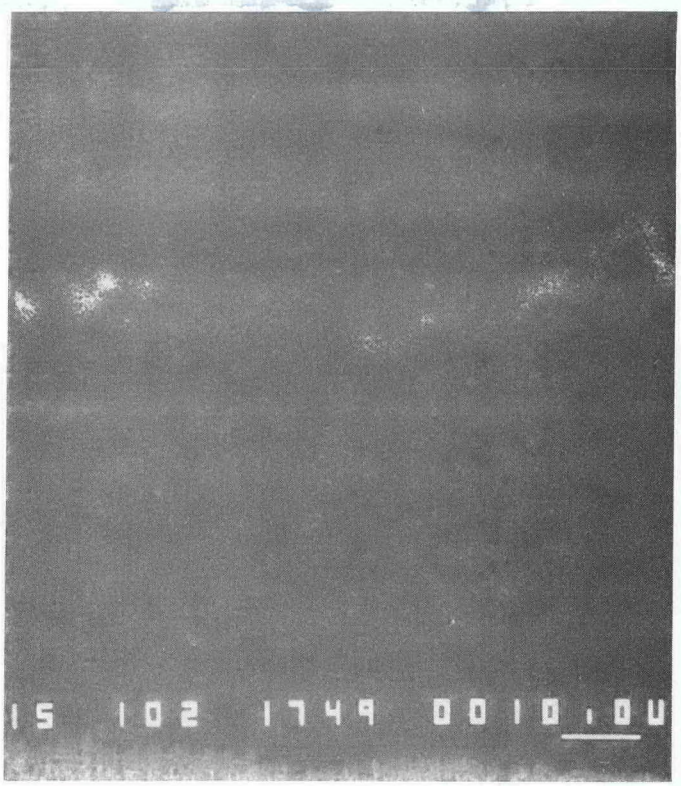

Sulfur

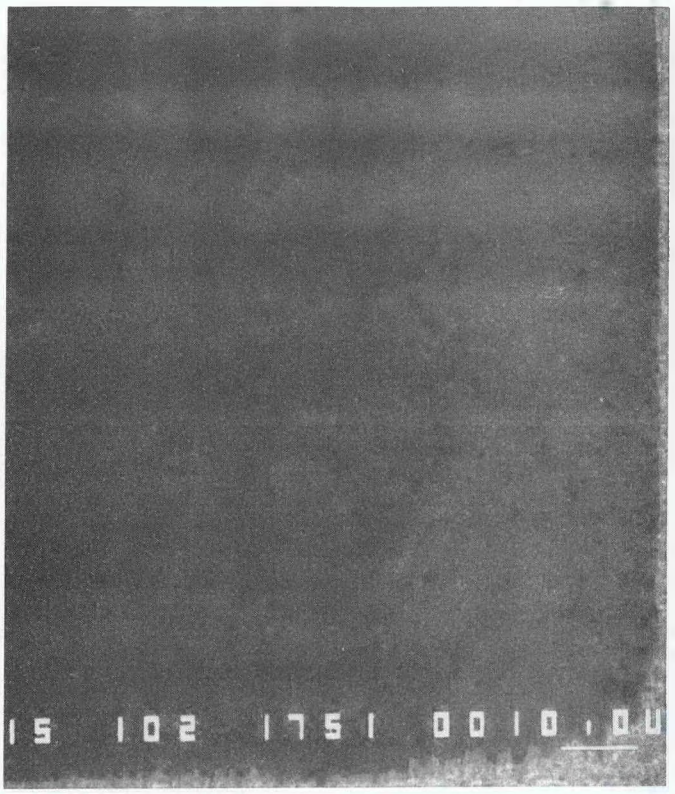

Potassium

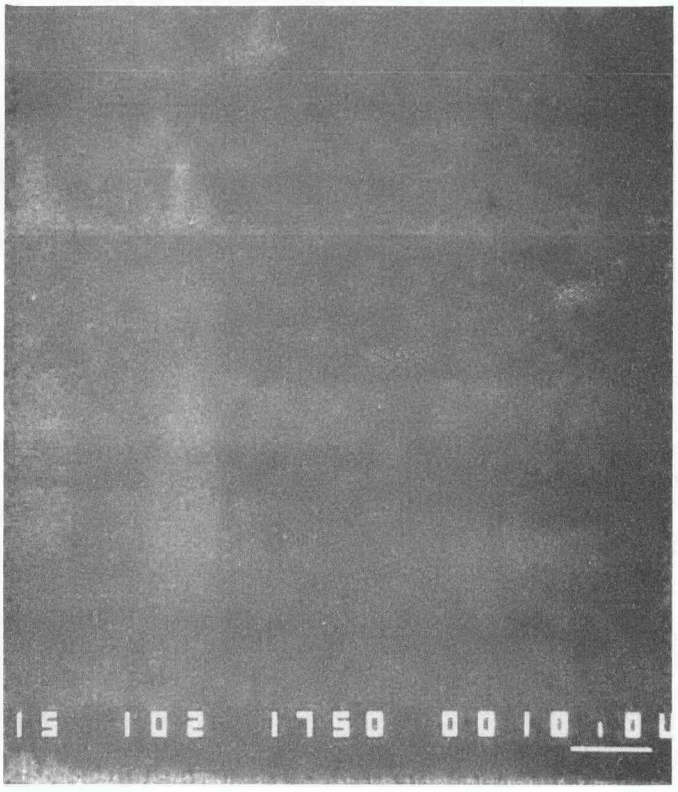

Chlorine

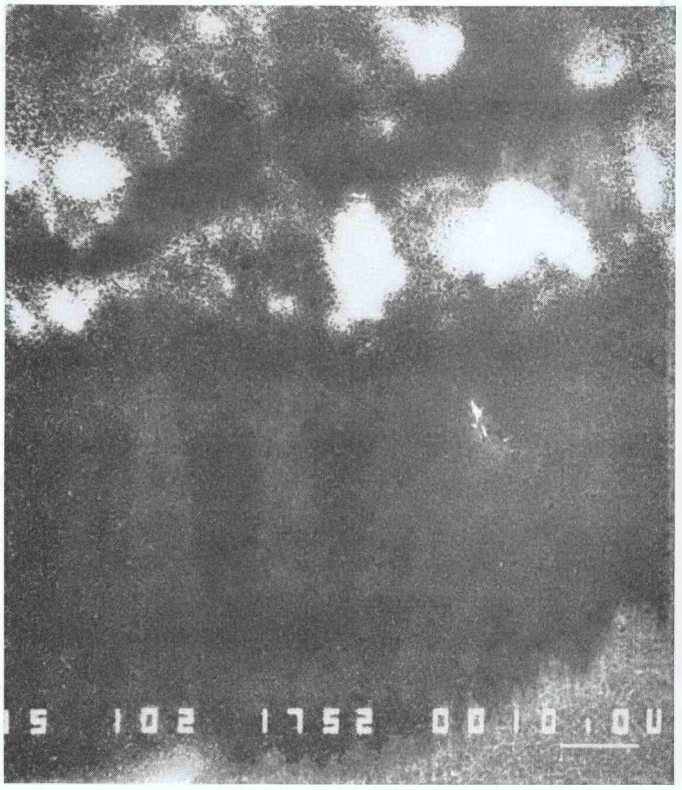

Calcium

FIGURE 15-B

XRF Element Maps of Cross Section of Wasted Region
of Tubing Sample 27-A-4

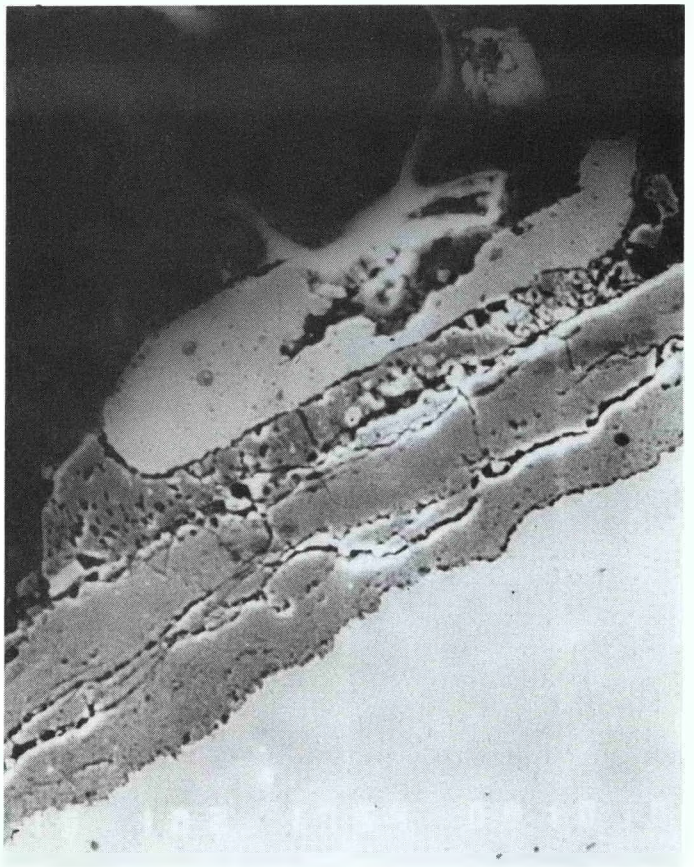

FIGURE 16-A

Cross Section at Top-Side of Tubing Sample 10-3-105
(SEM Secondary Electron Image of Area Used for XRF Maps of Figure 16-B)

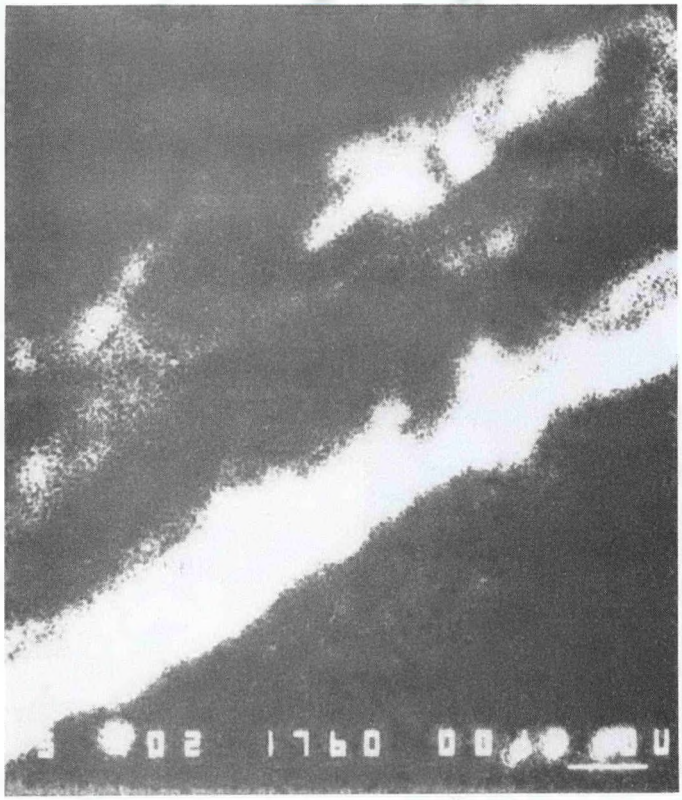

Sulfur

Potassium

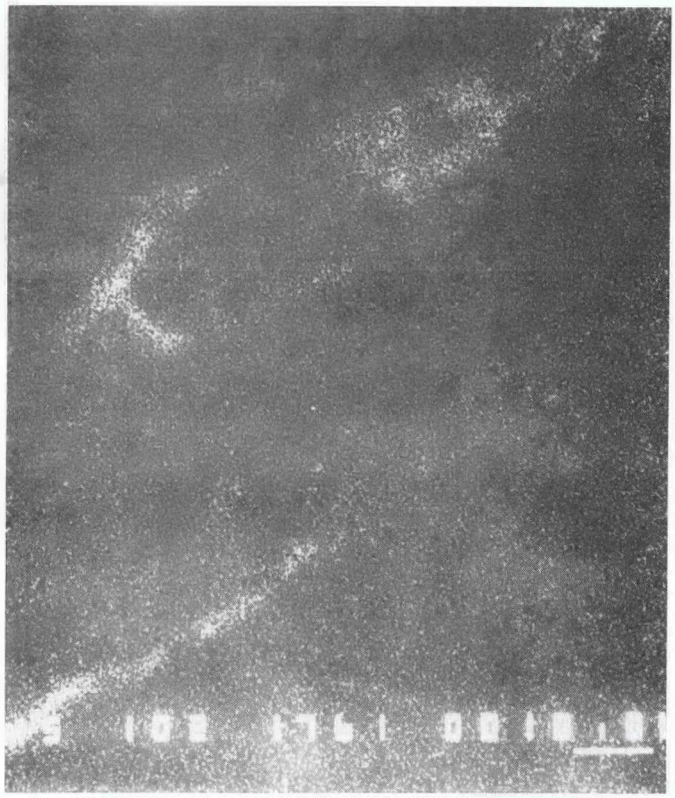

Chlorine

Calcium

FIGURE 16-B

XRF Element Maps of Cross Section at Top-Side
of Tubing Sample 10-3-105

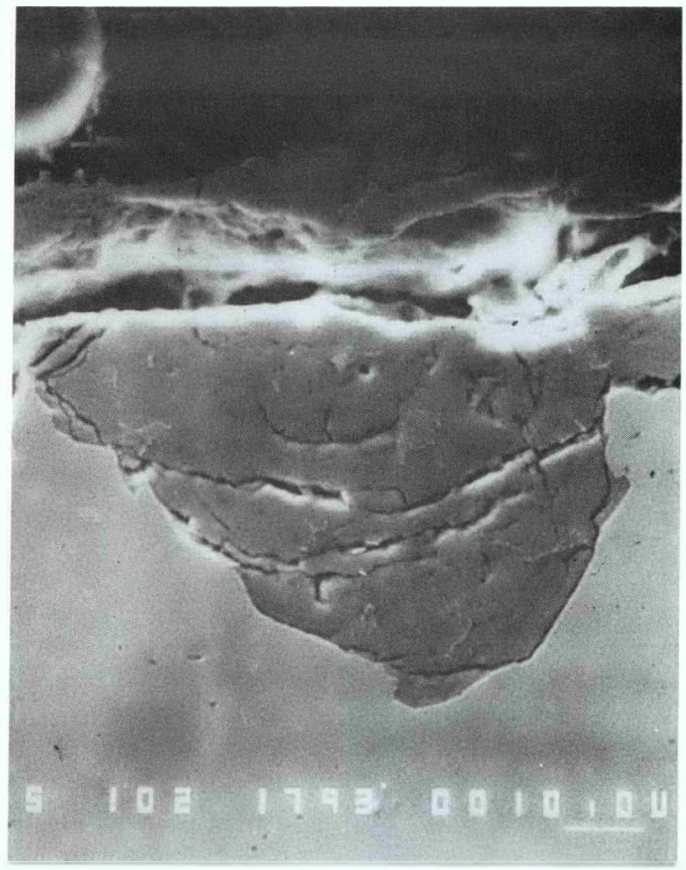

FIGURE 17-A

Cross Section at Underside of Tubing Sample 10-3-105
(SEM Secondary Electron Image of Area Used for XRF Maps of Figure 17-B)

Sulfur

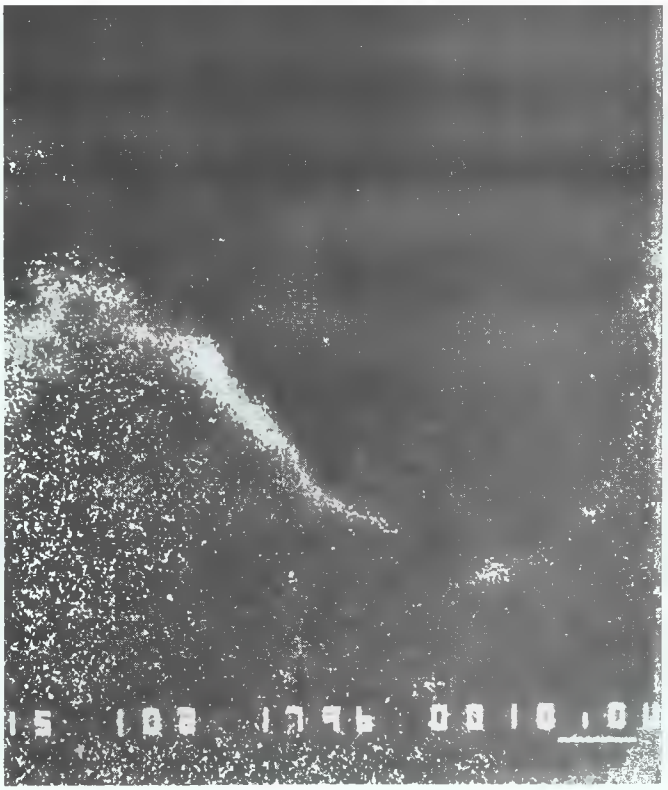

Potassium

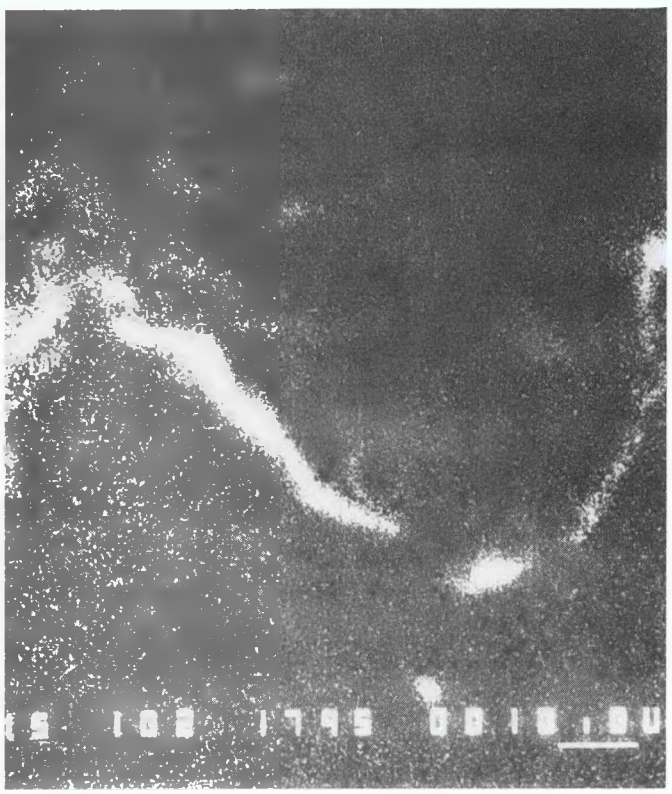

Chlorine

Calcium

FIGURE 17-B

XRF Element Maps of Cross Section at Top-Side
of Tubing Sample 10-3-105

Tubing Sample 8-1

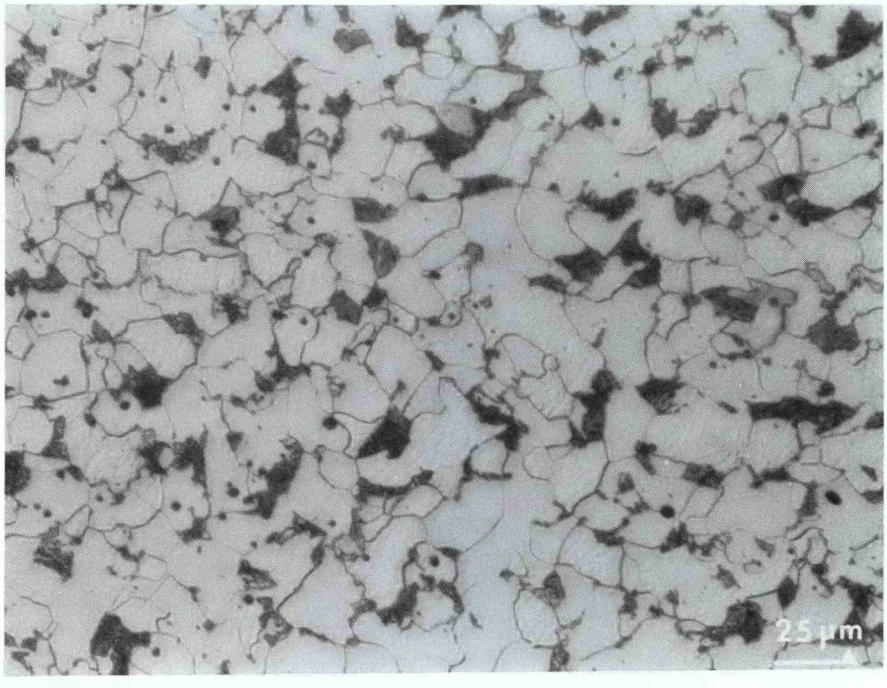

Tubing Sample 10-3-105

FIGURE 18

Microstructures of Steel Evaporator Tubes from Two Tube Banks
Experiencing Different Wastage Response
(Optical Photomicrographs, Etchant: 2% Nital)

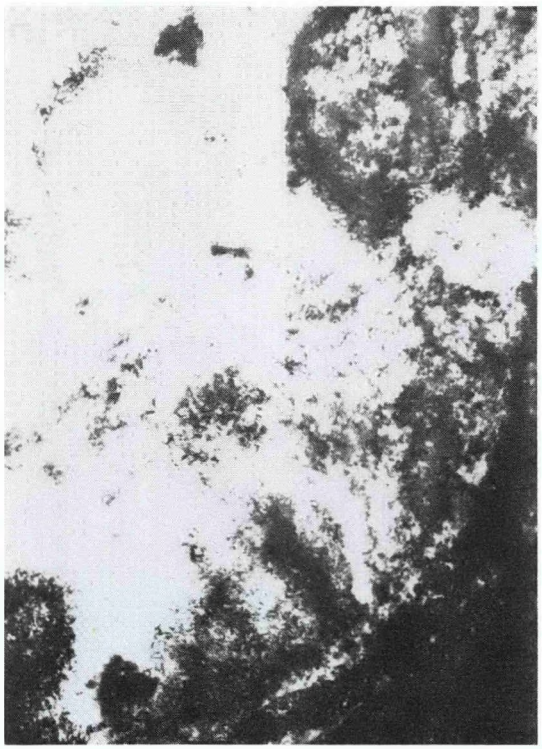

Wasted Region at Fireside Surface
(0.5 micron depth)

Reference Material from Tube Wall
in Non-Wasted Region but Located
at Same Radial Distance from Tube Axis
as Wasted Surface

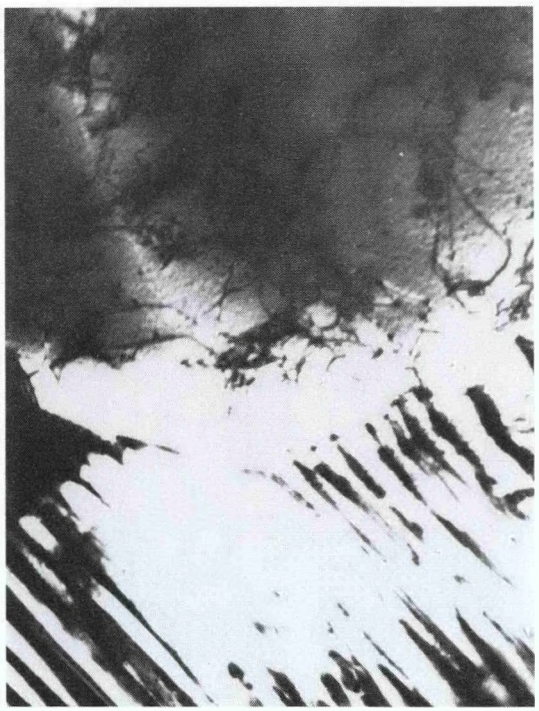

Non-Wasted Region at Fireside Surface
(0.5 micron depth)

FIGURE 19

TEM Microstructures of Tubing Sample 8-1
(Magnification: about 50,000x)

Figure 20
INDENTATION HARDNESS OF
EVAPORATOR TUBING STEELS

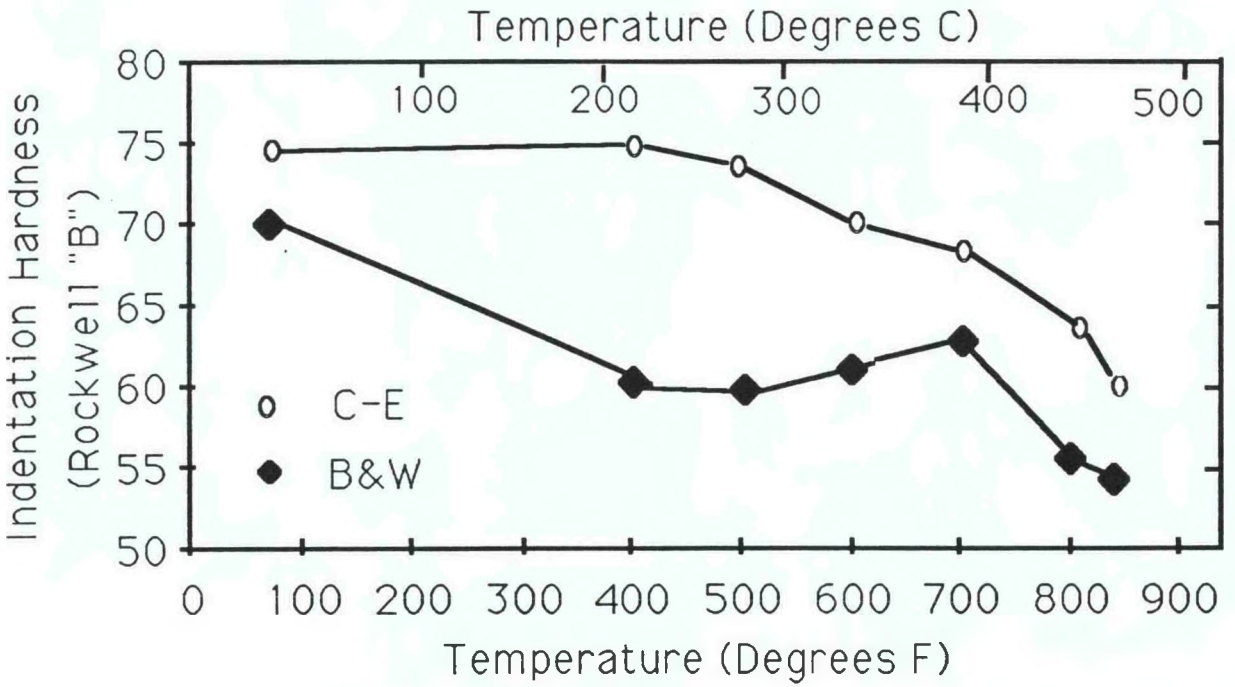

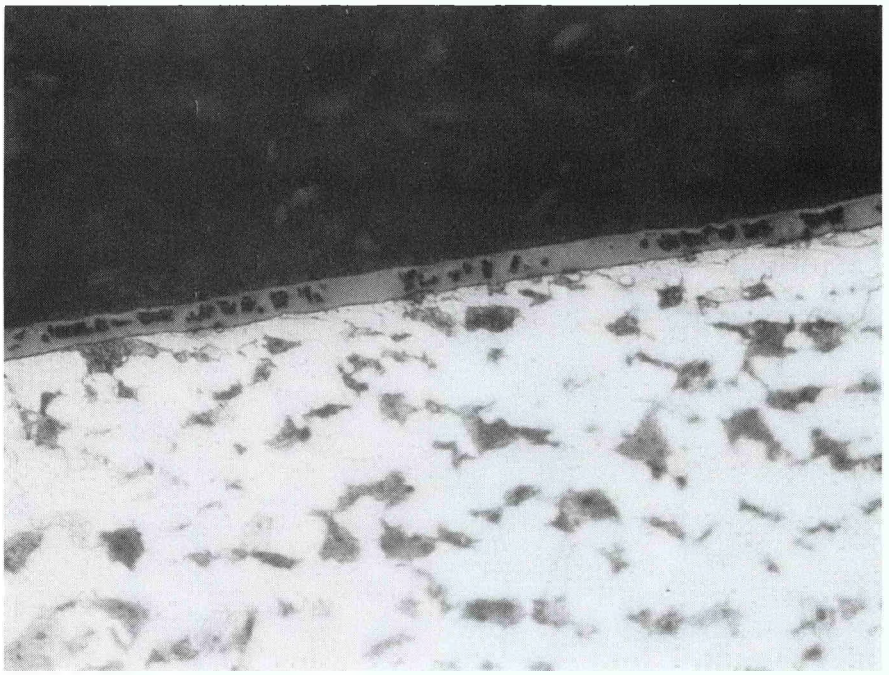

Etchant: 2% Nital 400x
Steel from Tubing Sample 8-1 (C-E)

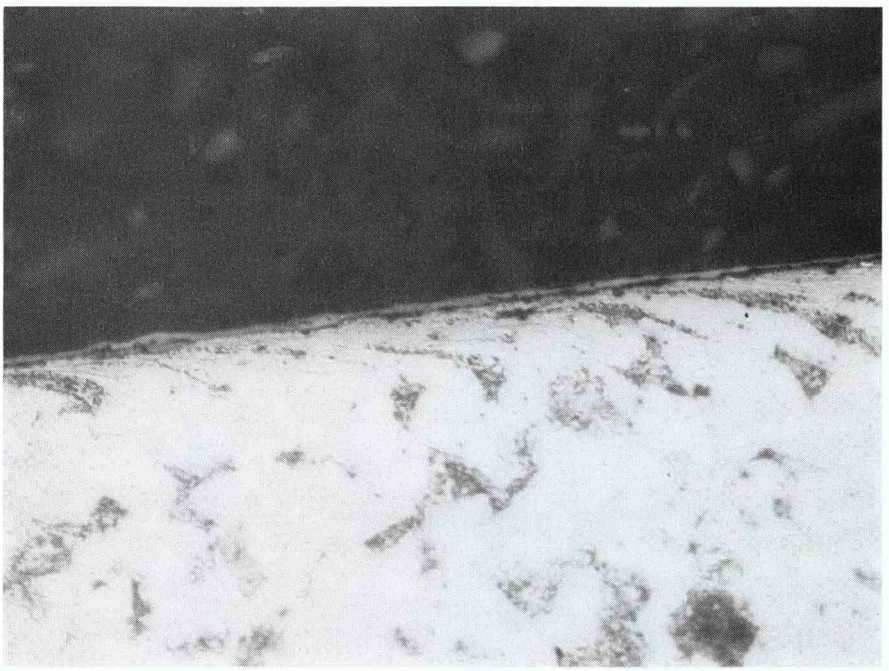

Etchant: 2% Nital 400x
Steel from Tubing Sample 10-3-105 (B&W)

FIGURE 21

Cross Sections of Tubing Steel Showing the Scale/Substrate Interface after Laboratory Oxidation Test at 450 C (Optical Photomicrographs)

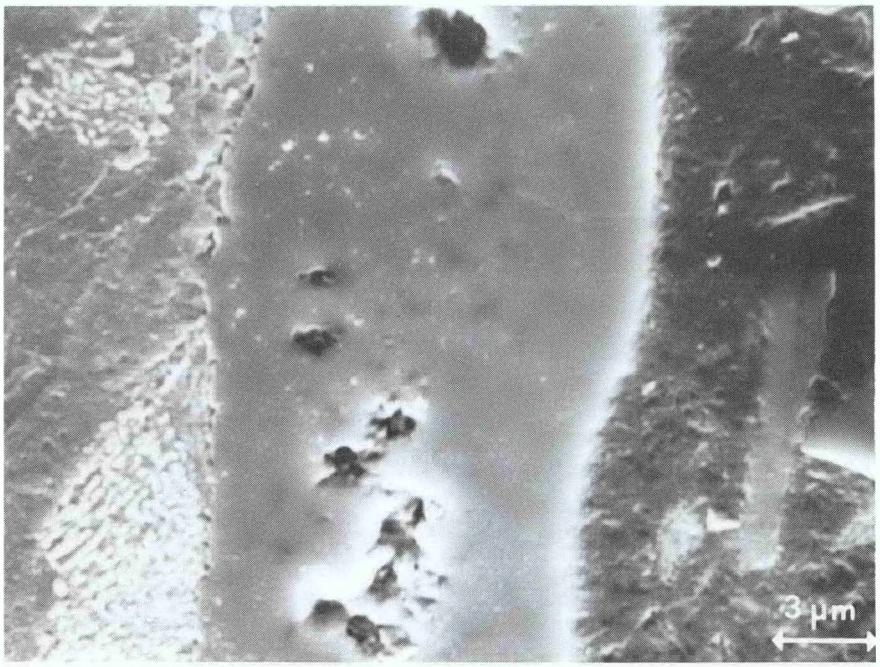

Steel from Tubing Sample 8-1 (C-E)

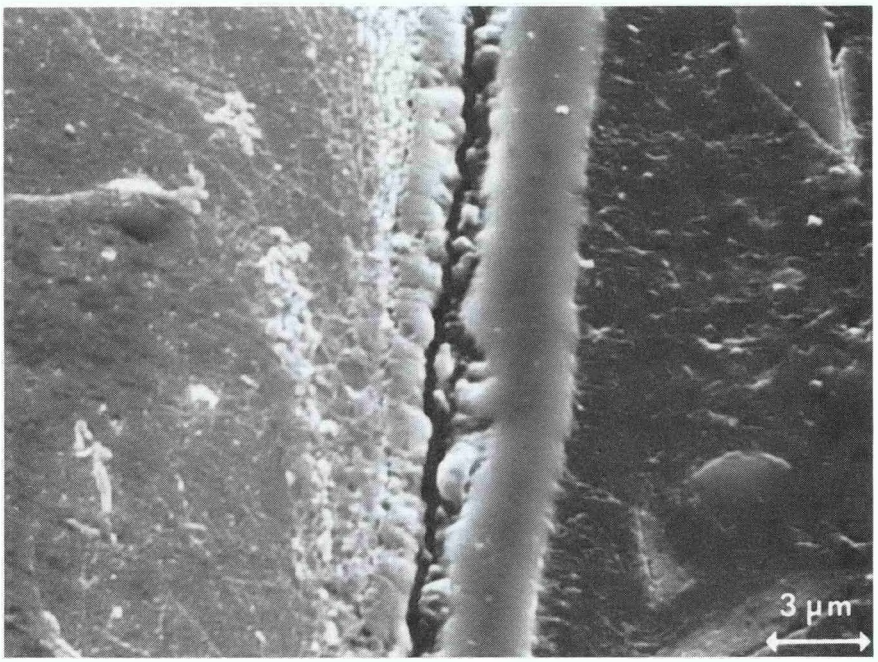

Steel from Tubing Sample 10-3-105 (B&W)

FIGURE 22

Cross Sections of Tubing Steel Showing the Scale/Substrate Interface after Laboratory Oxidation Test at 450 C (SEM Photomicrographs, Etchant: 2% Nital)

11.0 LIST OF ACRONYMS AND ABBREVIATIONS

AES	Auger Electron Spectroscopy
AFBC	Atmospheric Fluidized-Bed Combustor
B&W	Babcock & Wilcox Company
C-E	Combustion Engineering, Inc.
DOE	U. S. Department of Energy
EDS	Energy-Dispersive Spectroscopy
EMP	Electron Micro-Probe
EPRI	Electric Power Research Institute
FBC	Fluidized-Bed Combustor
IEA	International Energy Agency (UK)
LLNL	Lawrence Livermore National Laboratory
METC	Morgantown Energy Technology Center (DOE)
PFBC	Pressurized Fluidized-Bed Combustor
SEI	Secondary Electron Image
SEM	Scanning Electron Microscopy
TEM	Transmission Electron Microscopy
TVA	Tennessee Valley Authority
UK	United Kingdom
XPS	X-Ray Photoelectron Spectroscopy
XRF	X-Ray Fluorescence